Railway Engineering Science
https://doi.org/10.1007/s40534-024-00346-4

Integration of a hybrid vibration prediction model for railways into noise mapping software: methodology, assumptions and demonstration

Pieter Reumers[1] · Geert Degrande[1] · Geert Lombaert[1] · David J. Thompson[2] · Evangelos Ntotsios[2] · Pascal Bouvet[3] · Brice Nélain[3] · Andreas Nuber[4]

Received: 2 April 2024 / Revised: 7 June 2024 / Accepted: 10 June 2024

Abstract
Within the SILVARSTAR project, a user-friendly frequency-based hybrid prediction tool has been developed to assess the environmental impact of railway-induced vibration. This tool is integrated in existing noise mapping software. Following modern vibration standards and guidelines, the vibration velocity level in a building in each frequency band is expressed as the sum of a force density (source term), line source transfer mobility (propagation term) and building correction factor (receiver term). A hybrid approach is used that allows for a combination of experimental data and numerical predictions, providing increased flexibility and applicability. The train and track properties can be selected from a database or entered as numerical values. The user can select soil impedance and transfer functions from a database, pre-computed for a wide range of parameters with state-of-the-art models. An experimental database of force densities, transfer functions, free field vibration and input parameters is also provided. The building response is estimated by means of building correction factors. Assumptions within the modelling approach are made to reduce computation time but these can influence prediction accuracy; this is quantified for the case of a nominal intercity train running at different speeds on a ballasted track supported by homogeneous soil of varying stiffness. The paper focuses on the influence of these parameters on the compliance of the track–soil system and the free field response. We also demonstrate the use and discuss the validation of the vibration prediction tool for the case of a high-speed train running on a ballasted track in Lincent (Belgium).

Keywords Railway-induced vibration · Hybrid vibration prediction model · Experimental validation · Low-speed approximation

1 Introduction

Despite railway systems being a sustainable and climate-friendly mode of transport, noise and vibration remain particular environmental concerns. As urban congestion and demand for mass transport increase, new railways are being built in closer proximity to buildings, while building developments are expanding into areas surrounding existing railways. People living near railways are becoming increasingly sensitive and no longer accept noise and vibration annoyance, while the operation of sensitive equipment (e.g. electron microscopes, MRI scanners) is hampered by high levels of vibration. Yet, shifting more transport to rail can only be achieved with sustainable noise and vibration mitigation measures. The European Rail Research Advisory Council (EERAC) in its Strategic Rail Research and Innovation Agenda [1] has targeted 2050 as the year by which vibration and noise levels must be acceptable for 24-h railway operations.

In recent years, a wide variety of modelling approaches have been developed to assess the environmental impact of new railway lines or the extension of existing lines on the surrounding inhabitants [2, 3]. They involve a separation

✉ Pieter Reumers
pieter.reumers@kuleuven.be

1 Department of Civil Engineering, KU Leuven, Kasteelpark Arenberg 40, 3001 Leuven, Belgium

2 ISVR, University of Southampton, Highfield, Southampton SO17 1BJ, UK

3 Vibratec, 28 Chemin du petit bois, 69131 Ecully, France

4 Woelfel Engineering, GmbH + Co. K, Max-Planck Strasse 15, 97204 Hoechberg, Germany

Published online: 18 September 2024

into source, transmission and receiver terms [4] and can be divided into empirical, numerical or hybrid models.

- In empirical approaches, the source is described in terms of a force density [5] or a vibration spectrum on the ground close to the track. This was adopted in the empirical procedure for detailed vibration analysis proposed by the Federal Railroad Administration (FRA) and Federal Transit Administration (FTA) of the US Department of Transportation (DoT) [6, 7]. The vibration velocity level in a building, measured in decibels in one-third octave frequency bands, is written as a sum of a force density (source term), a line source transfer mobility (propagation term) and a building correction factor (receiver term).
- A wide range of numerical models have been developed for the prediction of vibration due to trains running at grade and in tunnels: (semi-)analytical models [8–11], 3D finite element (FE) [12–15], coupled finite element-boundary element (FE–BE) [16–18] and spectral element models [19], taking into consideration dynamic SSI at source and receiver, moving loads, as well as the longitudinal invariance or periodicity of the track–ground structure. A separation of the train–track–soil interaction problem into source, propagation and receiver terms is frequently used (e.g. for surface tracks [20] and tunnels [21, 22]). This resulted in different software tools, e.g. MOTIV [23–25], TRAFFIC [26], MEFISSTO [17] and the Pipe-in-Pipe model for trains running in tunnels [27–29].
- Hybrid models combine numerical prediction and experimental results. For each of the source, propagation or receiver terms, either measured data or a numerical model are used. Verbraken et al. [30] derived analytical expressions for the force density and the line source transfer mobility, while Kuo et al. [31, 32] used a hybrid model to predict railway-induced vibration in the free field and in a three-storey building. Vibratec's hybrid GroundVIB model [33] also combines numerical models with an experimental database.

Ground-borne noise and vibration studies are performed all around the world [34]. However, analysis is performed by simulation engineers, measurement specialists and academic researchers, using a wide range of models with different degrees of complexity and precision. Depending on the background and experience of a project team, a combination of in-house software, dedicated tools developed at universities or general purpose finite element programs may be used. A lack of uniformity and interfaces is observed, which does not facilitate the comparison of results obtained with different prediction models. Moreover, the quality of the predictions and the associated uncertainty strongly depend on the available data and the experience of the noise and vibration consultants involved. Existing models are not well integrated in the railway project development process. There is a general lack of user-friendly software incorporating widely accepted solution methods.

Therefore, the main novelty of this paper—aligned with one of the main objectives of the SILVARSTAR project [35]—is the development of a sufficiently fast-running, user-friendly and flexible hybrid vibration prediction tool that is based on a commonly accepted, practical and validated methodology. This hybrid vibration prediction model is integrated in existing noise mapping software, enabling engineers to perform noise and vibration analysis from railways at similar large spatial scales, within the same software environment. To achieve fast computation times, pre-computed soil impedance and transfer functions are made available, while several modelling assumptions are introduced without sacrificing too much in terms of prediction accuracy; the resulting insights, in their own, are also novel contributions. Furthermore, the hybrid vibration prediction tool is equipped with an experimental database obtained from well-documented case histories, and an open interface that will encourage future users to add more case histories. This is illustrated with a detailed case history of a high-speed ballasted track, which provides complementary insights in the performance of the model.

Following a presentation in Sect. 2 of the proposed methodology [36] that is based on modern vibration standards and guidelines [4, 6, 7], a frequency-based hybrid modelling approach is presented in Sect. 3. To ensure that the modelling approach is sufficiently efficient, various simplifying assumptions must be introduced, which influence prediction accuracy. In particular, the train speed and soil properties influence the compliance of the track–soil system, the dynamic axle loads and the free field response. The effect of these modelling assumptions on prediction accuracy is quantified in Sect. 4 for the case of a nominal intercity (IC) train running at different speeds on a ballasted track supported by homogeneous soil of varying stiffness. The use and validation of the hybrid vibration prediction tool are demonstrated in Sect. 5 for a high-speed train running on a ballasted track on high-speed line L2 in Lincent (Belgium). Conclusions are formulated in Sect. 6.

2 Methodology

2.1 General framework

The basic concept for the prediction of ground vibration in SILVARSTAR is to develop a frequency-based hybrid vibration prediction tool, following the general framework recommended in the ISO 14837-1:2005 standard

[4]. This standard expresses the quasi-stationary vibration level $A(f)$ in a building during a train passage as the product of a source term $S(f)$ for the vehicle–track interaction, a propagation term $P(f)$ for the soil and a receiver term $R(f)$ for the building:

$$A(f) = S(f)P(f)R(f). \tag{1}$$

The vibration level $A(f)$ typically is a root mean square value of velocity or acceleration in one-third octave bands; equivalently, it can also be expressed in decibels which transforms the product on the right-hand side of Eq. (1) into a summation of three terms.

The three terms on the right-hand side are evaluated at the same frequency f, which is strictly not valid for moving sources due to the Doppler effect [37]. It is expected to provide a reasonable estimate for the quasi-stationary response, however, when the train speed is relatively low compared with the wave velocities in the soil [38]. Each of the terms in Eq. (1) can be represented by numerical predictions or by experimental data.

2.2 Empirical prediction scheme

2.2.1 Vibration velocity level

The empirical procedure for Detailed Vibration Assessment proposed by the FRA/FTA of the US DoT [6, 7] conforms to the framework of ISO 14837-1:2005 [4] and is used as a basis for the development of a hybrid vibration prediction tool, allowing a combination of experimental and numerical results.

The vibration velocity level $L_v(\boldsymbol{x}_b)$ at a receiver $\boldsymbol{x}_b$ in the building (Fig. 1a) is defined as the root mean square (RMS) value of the velocity during the stationary part of a train passage; it is expressed in decibels (dB ref. 5×10^{-8} m/s) in one-third octave bands as a sum of source, propagation and receiver terms:

$$L_v(\boldsymbol{x}_b) = L_F(\boldsymbol{X}, \boldsymbol{x}_1) + \mathrm{TM}_L(\boldsymbol{X}, \boldsymbol{x}_1) + C_b(\boldsymbol{x}_1, \boldsymbol{x}_b). \tag{2}$$

The first term $L_F(\boldsymbol{X}, \boldsymbol{x}_1)$ is the equivalent force density (dB ref. $1\,\mathrm{N}/\sqrt{\mathrm{m}}$). The vector $\boldsymbol{X}$ collects all the source points, located on the rail heads, while the receivers $\boldsymbol{x}_1$ are located on the ground surface. The second term $\mathrm{TM}_L(\boldsymbol{X}, \boldsymbol{x}_1)$ is the line source transfer mobility (dB ref. 5×10^{-8} (m/s)/(N/$\sqrt{\mathrm{m}}$)). The third term $C_b(\boldsymbol{x}_1, \boldsymbol{x}_b)$ is the receiver term or the building correction factor; it is computed as a combination of adjustment factors to account for dynamic soil–structure interaction (SSI) at foundation level and attenuation and amplification within the building. These three terms are explained in the following subsections.

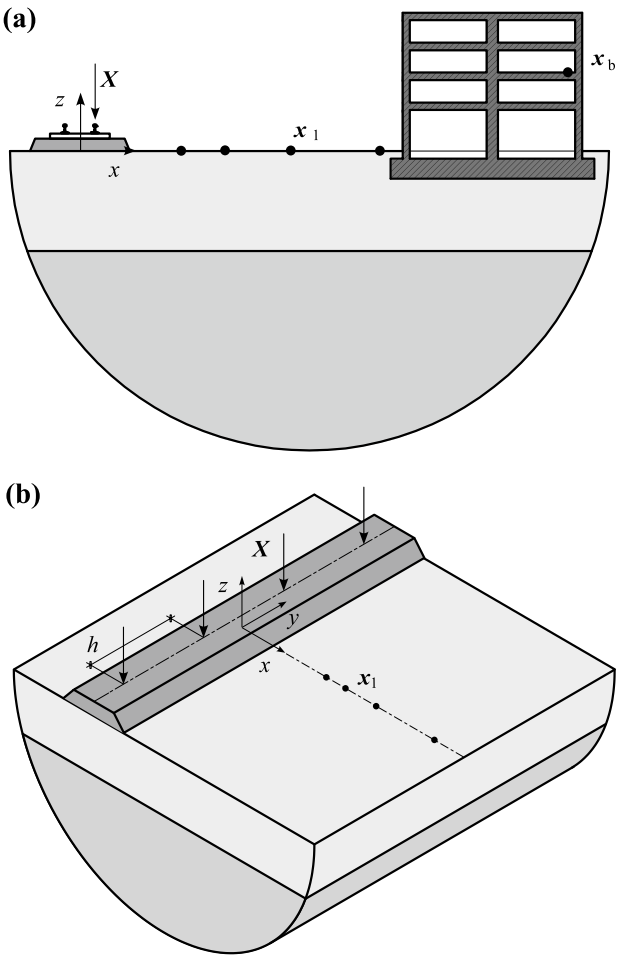

Fig. 1 Source and receiver points **a** for the FRA procedure and **b** for line source transfer mobility measurements

2.2.2 Line source transfer mobility (LSTM)

The line source transfer mobility (LSTM) $\mathrm{TM}_L(\boldsymbol{X}, \boldsymbol{x}_1)$ is derived from the superposition of point source transfer mobilities $\mathrm{TM}_P(\boldsymbol{X}_k, \boldsymbol{x}_1)$ for a series of n equidistant source points $\boldsymbol{X}_k$ with spacing h [6, 7, 37]:

$$\mathrm{TM}_L(\boldsymbol{X}, \boldsymbol{x}_1) = 10 \log_{10} \left[h \sum_{k=1}^{n} 10^{\frac{\mathrm{TM}_P(\boldsymbol{X}_k, \boldsymbol{x}_1)}{10}} \right]. \tag{3}$$

Fig. 1b shows a measurement setup for vibration propagation tests with a track at grade. Impacts are given at equally spaced points $\boldsymbol{X}$ along the track, and the resulting vibration velocity is measured at a receiver $\boldsymbol{x}_1$ on a line perpendicular to the track. The point source transfer mobility $\mathrm{TM}_P(\boldsymbol{X}_k, \boldsymbol{x}_1)$ is determined in one-third octave bands. For the case of a new railway, source points $\boldsymbol{X}$ at the rail heads are not available, so alternative impact locations on the soil's surface close to the future track position are used. A similar procedure is applied for a track in a tunnel, where impacts are

given on the rail head or in a borehole if a tunnel has not yet been built.

Alternative choices for the distribution of loads along the track and impact locations (single or both rail heads, sleeper centre or edge) are discussed by Verbraken [37]. Assuming equidistant source points $\boldsymbol{X}$ along the track instead of the actual axle positions mainly affects the LSTM at high frequencies for receivers close to the track; when the spacing h is sufficiently small (we use 10 m to 12 m in measurement campaigns), the influence can be limited to around 3 dB. Furthermore, the source points $\boldsymbol{X}$ can be applied at both rails or at the sleeper centre, yielding almost identical results. If applied at one rail or the sleeper edge, the rotation of the sleeper results in higher values (around 6 dB) of the LSTM at high frequencies when the wavelength in the soil approaches the sleeper length.

2.2.3 Force density

If the building's coupling loss term is omitted from Eq. (2), the expression for the vibration velocity level at a receiver $\boldsymbol{x}_1$ located in the free field, still in presence of the building, is given as

$$L_{\mathrm{v}}(\boldsymbol{x}_1) = L_{\mathrm{F}}(\boldsymbol{X},\boldsymbol{x}_1) + \mathrm{TM}_{\mathrm{L}}(\boldsymbol{X},\boldsymbol{x}_1). \tag{4}$$

Depending on the location of the receiver $\boldsymbol{x}_1$ with respect to the building, this may include the effect of dynamic SSI. Rearranging Eq. (4) gives a method of determining the force density $L_{\mathrm{F}}(\boldsymbol{X},\boldsymbol{x}_1)$ indirectly:

$$L_{\mathrm{F}}(\boldsymbol{X},\boldsymbol{x}_1) = L_{\mathrm{v}}(\boldsymbol{x}_1) - \mathrm{TM}_{\mathrm{L}}(\boldsymbol{X},\boldsymbol{x}_1). \tag{5}$$

This excitation force term represents the equivalent fixed line source that results in the same vibration velocity level as the train passage. The force density $L_{\mathrm{F}}(\boldsymbol{X},\boldsymbol{x}_1)$ depends on the actual force generated at the wheel/rail interface and the dynamic characteristics of the transit structure, including the track, subgrade and soil. Apart from the source positions $\boldsymbol{X}$ used for the determination of the LSTM, it also depends on receiver positions $\boldsymbol{x}_1$ at which the vibration velocity level $L_{\mathrm{v}}(\boldsymbol{x}_1)$ and LSTM $\mathrm{TM}_{\mathrm{L}}(\boldsymbol{X},\boldsymbol{x}_1)$ are subtracted.

2.2.4 Building correction factor

The building correction factor $C_{\mathrm{b}}(\boldsymbol{x}_1,\boldsymbol{x}_{\mathrm{b}})$ can be quantified as a difference between the vibration velocity level $L_{\mathrm{v}}(\boldsymbol{x}_{\mathrm{b}})$ at a point $\boldsymbol{x}_{\mathrm{b}}$ in the building and $L_{\mathrm{v}}(\boldsymbol{x}_1)$ at a point $\boldsymbol{x}_1$ on the ground surface with the building present (Fig. 1a):

$$C_{\mathrm{b}}(\boldsymbol{x}_1,\boldsymbol{x}_{\mathrm{b}}) = L_{\mathrm{v}}(\boldsymbol{x}_{\mathrm{b}}) - L_{\mathrm{v}}(\boldsymbol{x}_1). \tag{6}$$

The vibration velocities are determined by measurements during a train passage. The building correction factor depends on the positions of $\boldsymbol{x}_1$ and $\boldsymbol{x}_{\mathrm{b}}$ relative to the track. The closer $\boldsymbol{x}_1$ is to the building, the more the vibration level $L_{\mathrm{v}}(\boldsymbol{x}_1)$ is influenced by the presence of the building. Locating the receiver $\boldsymbol{x}_1$ far from the building results in a coupling loss that includes a greater contribution from the propagation path. The position $\boldsymbol{x}_{\mathrm{b}}$ can vary within the building and determines whether the receiver term incorporates effects such as floor-to-floor attenuation and floor resonances.

The definition of the building correction factor is further elaborated by expressing the two vibration velocity levels as the sum of excitation force and propagation path terms. For example, writing

$$L_{\mathrm{v}}(\boldsymbol{x}_{\mathrm{b}}) = L_{\mathrm{F}}(\boldsymbol{X},\boldsymbol{x}_{\mathrm{b}}) + \mathrm{TM}_{\mathrm{L}}(\boldsymbol{X},\boldsymbol{x}_{\mathrm{b}}), \tag{7}$$

and incorporating Eq. (4) for $L_{\mathrm{v}}(\boldsymbol{x}_1)$ results in the following building correction factor

$$\begin{aligned} C_{\mathrm{b}}(\boldsymbol{x}_1,\boldsymbol{x}_{\mathrm{b}}) = {} & \mathrm{TM}_{\mathrm{L}}(\boldsymbol{X},\boldsymbol{x}_{\mathrm{b}}) - \mathrm{TM}_{\mathrm{L}}(\boldsymbol{X},\boldsymbol{x}_1) \\ & + L_{\mathrm{F}}(\boldsymbol{X},\boldsymbol{x}_{\mathrm{b}}) - L_{\mathrm{F}}(\boldsymbol{X},\boldsymbol{x}_1). \end{aligned} \tag{8}$$

By assuming the two force densities to be equal, the building correction factor is approximately written as

$$C_{\mathrm{b}}(\boldsymbol{x}_1,\boldsymbol{x}_{\mathrm{b}}) \simeq \mathrm{TM}_{\mathrm{L}}(\boldsymbol{X},\boldsymbol{x}_{\mathrm{b}}) - \mathrm{TM}_{\mathrm{L}}(\boldsymbol{X},\boldsymbol{x}_1). \tag{9}$$

This calculation of the building correction factor only depends on the difference between the LSTMs measured at a point $\boldsymbol{x}_{\mathrm{b}}$ in the building and at a point $\boldsymbol{x}_1$ on the ground surface in the presence of the building. It does not require the passage of a train, making it a useful means of measuring the building correction factor in the field, provided that the excitation applied at $\boldsymbol{X}$ is sufficiently large to produce a measurable building response. It also simplifies a numerical computation of the building response by removing the need for a vehicle model and characterization of the wheel–rail unevenness.

Different options to quantify building correction factors are discussed in Sect. 3.3.

2.2.5 Source characterization by means of reference ground vibration level

According to ISO 14837-1:2005 [4], the source term may be "a forcing function at the wheel/rail interface or, alternatively, may be a vibration response (velocity or acceleration) at a defined location (e.g. tunnel invert, tunnel wall or in the ground to the side of the tunnel or to the side of the track at grade)". In Germany and the Netherlands, it is common practice to use a vibration velocity level $L_{\mathrm{v}}(\boldsymbol{x}_{\mathrm{ref}})$ at a reference distance $\boldsymbol{x}_{\mathrm{ref}}$ from surface tracks of, respectively, 8 m and 25 m [39]. This alternative is therefore also provided, although it is definitely preferable to represent the source term as a force at the wheel/rail interface, as this source term is less sensitive to local soil conditions.

When Eq. (2) is evaluated for both $L_v(\boldsymbol{x}_1)$ and $L_v(\boldsymbol{x}_{ref})$, the former can be expressed as

$$\begin{aligned} L_v(\boldsymbol{x}_1) = {} & L_v(\boldsymbol{x}_{ref}) + L_F(\boldsymbol{X},\boldsymbol{x}_1) - L_F(\boldsymbol{X},\boldsymbol{x}_{ref}) \\ & + \mathrm{TM}_L(\boldsymbol{X},\boldsymbol{x}_1) - \mathrm{TM}_L(\boldsymbol{X},\boldsymbol{x}_{ref}). \end{aligned} \tag{10}$$

If it is assumed that the force densities $L_F(\boldsymbol{X},\boldsymbol{x}_{ref})$ and $L_F(\boldsymbol{X},\boldsymbol{x}_1)$ are equal, Eq. (10) is approximated as

$$\begin{aligned} L_v(\boldsymbol{x}_1) \simeq {} & L_v(\boldsymbol{x}_{ref}) + \underline{\mathrm{TM}_L(\boldsymbol{X},\boldsymbol{x}_1) - \mathrm{TM}_L(\boldsymbol{X},\boldsymbol{x}_{ref})} \\ = {} & L_v(\boldsymbol{x}_{ref}) + \Delta\mathrm{TM}_L(\boldsymbol{X},\boldsymbol{x}_1,\boldsymbol{x}_{ref}). \end{aligned} \tag{11}$$

The underlined term represents the difference in LSTMs $\Delta\mathrm{TM}_L(\boldsymbol{X},\boldsymbol{x}_1,\boldsymbol{x}_{ref})$ at the receivers $\boldsymbol{x}_1$ and $\boldsymbol{x}_{ref}$, for excitation at source locations $\boldsymbol{X}$.

2.3 Numerical prediction scheme using a modular approach

2.3.1 State-of-the-art numerical models

The state-of-the-art models MOTIV [23–25] and TRAFFIC [26] have been used as a basis for further development, verification and approval testing. Both models are based on the following general expression for the time history $u_i(\boldsymbol{x},t)$ of the displacement at a receiver $\boldsymbol{x}$ due to n_a axle loads $g_{kj}(t)$ $(k = 1,2,\ldots,n_a)$ moving with constant speed v in the direction $\boldsymbol{e}_y$:

$$u_i(\boldsymbol{x},t) = \sum_{k=1}^{n_a} \int_{-\infty}^{t} h_{ji}(\boldsymbol{x}_k(\tau),\boldsymbol{x},t-\tau) g_{kj}(\tau)\,\mathrm{d}\tau. \tag{12}$$

The transfer function (or impulse response function) $h_{ij}(\boldsymbol{x}',\boldsymbol{x},t)$ represents the displacement at a point $\boldsymbol{x}$ in the direction $\boldsymbol{e}_j$ at time t due to an impulse load at a point $\boldsymbol{x}'$ in the direction $\boldsymbol{e}_i$ at time $t = 0$. The axle load $g_{kj}(t) = g_{skj} + g_{dkj}(t)$ is decomposed in a quasi-static component and a dynamic component (and often assumed to act in the vertical direction). $\boldsymbol{x}_k(t) = \boldsymbol{x}_{k0} + vt\boldsymbol{e}_y$ is the time-dependent position of the k-th axle load with initial position $\boldsymbol{x}_{k0}$. The response $\hat{u}_i(\boldsymbol{x},\omega)$ in the frequency domain is calculated as the forward Fourier transform from the time t to the circular frequency ω:

$$\hat{u}_i(\boldsymbol{x},\omega) = \sum_{k=1}^{n_a} \int_{-\infty}^{t} \hat{h}_{ji}(\boldsymbol{x}_k(\tau),\boldsymbol{x},\omega) g_{kj}(\tau) \exp(-\mathrm{i}\omega\tau)\,\mathrm{d}\tau, \tag{13}$$

where a hat on a variable denotes its representation in the spatial-frequency domain, and i is the imaginary unit.

Assuming that both the track and soil are invariant in the direction $\boldsymbol{e}_y$ along the track, the response in the wavenumber-frequency domain is

$$\begin{aligned} & \tilde{u}_i(x,k_y,z,\omega) \\ & = \sum_{k=1}^{n_a} \tilde{h}_{ji}(x,k_y,z,\omega)\hat{g}_{kj}(\omega - k_y v)\exp(+\mathrm{i}k_y y_{k0}), \end{aligned} \tag{14}$$

where a tilde on a variable denotes its representation in the wavenumber-frequency domain. The response in the spatial-frequency domain is obtained as the inverse Fourier transform from the wavenumber k_y to the coordinate y:

$$\begin{aligned} \hat{u}_i(x,y,z,\omega) = \sum_{k=1}^{n_a} \frac{1}{2\pi} \int_{-\infty}^{+\infty} & \tilde{h}_{ji}(x,k_y,z,\omega)\hat{g}_{kj}(\omega - k_y v) \\ & \times \exp\left[-\mathrm{i}k_y(y - y_{k0})\right] \mathrm{d}k_y. \end{aligned} \tag{15}$$

The frequency shift on the dynamic axle load represents the Doppler effect. A change of variables according to $k_y = (\omega - \tilde{\omega})/v$ moves this frequency shift from the frequency content of the moving load to the wavenumber content of the transfer function:

$$\begin{aligned} \hat{u}_i(x,y,z,\omega) = \sum_{k=1}^{n_a} \frac{1}{2\pi v} \int_{-\infty}^{+\infty} & \tilde{h}_{ji}\left(\frac{\omega - \tilde{\omega}}{v},\omega\right)\hat{g}_{kj}(\tilde{\omega}) \\ & \times \exp\left[-\mathrm{i}\frac{\omega - \tilde{\omega}}{v}(y - y_{k0})\right] \mathrm{d}\tilde{\omega}. \end{aligned} \tag{16}$$

The response in the spatial-time domain is subsequently obtained by an inverse Fourier transformation.

The above derivations demonstrate that the response of a coupled track–soil system is obtained once the system's transfer function and the axle loads are computed. If the track–soil system is three-dimensional (3D), then Eqs. (12) or (13) must be solved. If it can be assumed that the geometry is invariant in the direction $\boldsymbol{e}_y$ along the track, then the two-and-a-half dimensional (2.5D) Eqs. (15) or (16) offer a more efficient alternative. Both MOTIV and TRAFFIC models follow the latter approach in the wavenumber-frequency domain (Fig. 2). They couple a semi-analytical track model, consisting of beams, masses, springs and dampers (representing the rails, rail pads, base plates, sleepers, under sleeper pads and ballast or slab) to a boundary element (BE) model representing a layered soil. Different kinematic assumptions are made at the track–soil interface: MOTIV models arbitrary displacement patterns, whereas TRAFFIC applies a modal reduction imposing rigid body kinematics in terms of the centre's vertical displacement and rotation. Both models compute the soil's impedance matrix that is coupled to the track model, as well as transfer functions to any output location on the track or in the soil (the so-called free field).

When the geometry is invariant in the direction $\boldsymbol{e}_y$, the dynamic axle loads $\hat{\boldsymbol{g}}_d(\omega)$ are computed as [26, 36, 40]

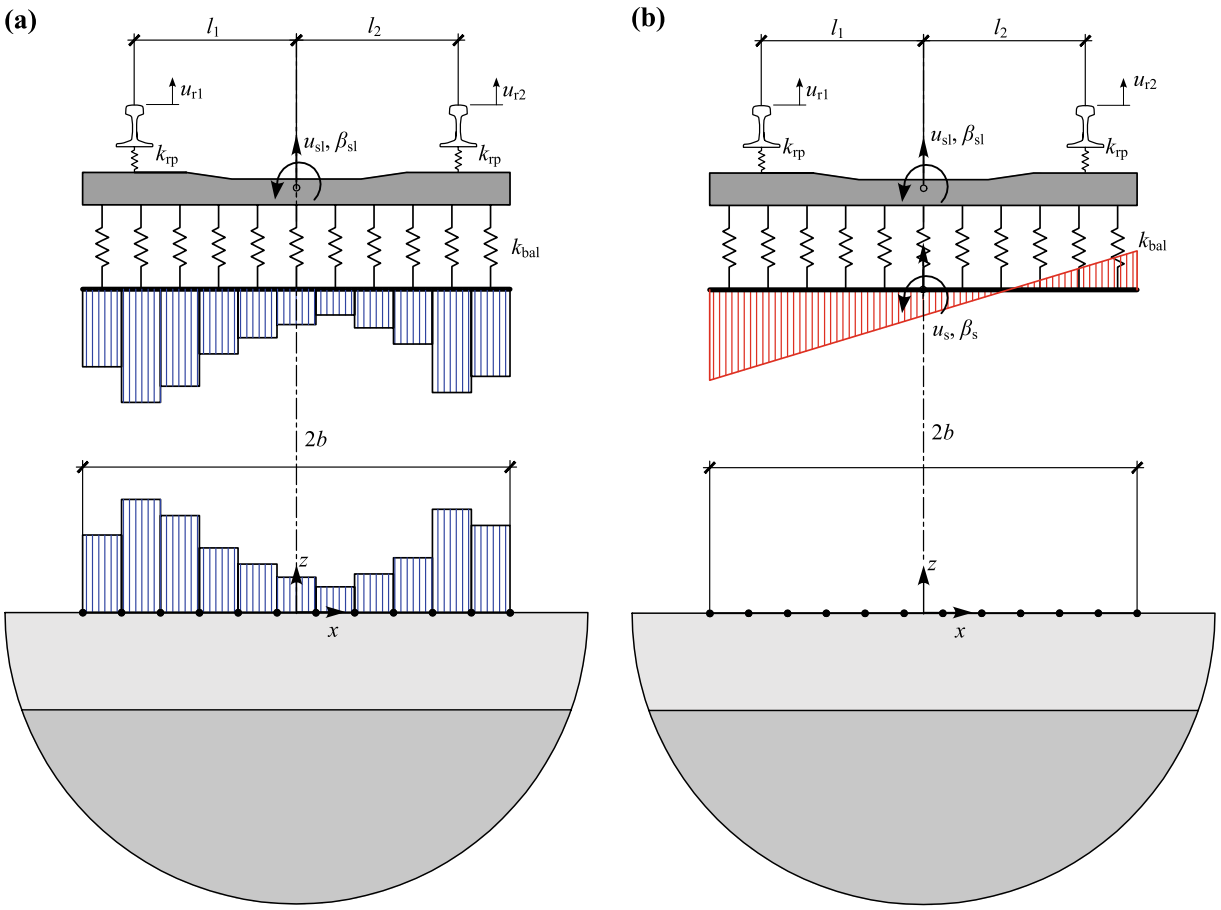

Fig. 2 Cross section of the semi-analytical track model coupled to a layered soil in the models: **a** MOTIV (tractions in blue); **b** TRAFFIC (rigid body displacements in red). The variables are explained in Table 2

$$\left[\boldsymbol{C}^{\mathrm{t}}(\omega)+\boldsymbol{C}^{\mathrm{v}}(\omega)\right]\hat{\boldsymbol{g}}_{\mathrm{d}}(\omega)=-\hat{\boldsymbol{u}}_{\mathrm{w/r}}(\omega), \tag{17}$$

where $\boldsymbol{C}^{\mathrm{t}}(\omega)$ is the track compliance matrix, $\boldsymbol{C}^{\mathrm{v}}(\omega)$ is the vehicle compliance matrix and $\hat{\boldsymbol{u}}_{\mathrm{w/r}}(\omega)$ is the combined wheel and rail unevenness perceived by each of the axles. The elements $\hat{C}^{\mathrm{t}}_{kl}(\omega)$ of the track compliance matrix $\boldsymbol{C}^{\mathrm{t}}(\omega)$ correspond to the vertical displacement at the position of axle l due to a unit vertical load at the position of axle k, and are calculated from a reformulation of Eq. (15) in a moving frame of reference $\hat{\boldsymbol{x}}=\{x,\hat{y},z\}^{\mathrm{T}}$ with $\hat{y}=y-vt$:

$$\hat{C}^{\mathrm{t}}_{kl}(\omega)=\frac{1}{2\pi}\int_{-\infty}^{+\infty}\tilde{h}^{\mathrm{t}}_{zz}(k_y,\omega+k_y v)\exp\left[-\mathrm{i}k_y(y_{l0}-y_{k0})\right]\mathrm{d}k_y, \tag{18}$$

where $\tilde{h}^{\mathrm{t}}_{zz}(k_y,\omega+k_y v)$ denotes the transfer function of the track–soil system in the wavenumber-frequency domain in a moving frame of reference. The vehicle is modelled as a multi-degree of freedom (MDOF) system, where the car body, bogies and wheelsets are considered as rigid parts, characterized by their mass and mass moment of inertia,

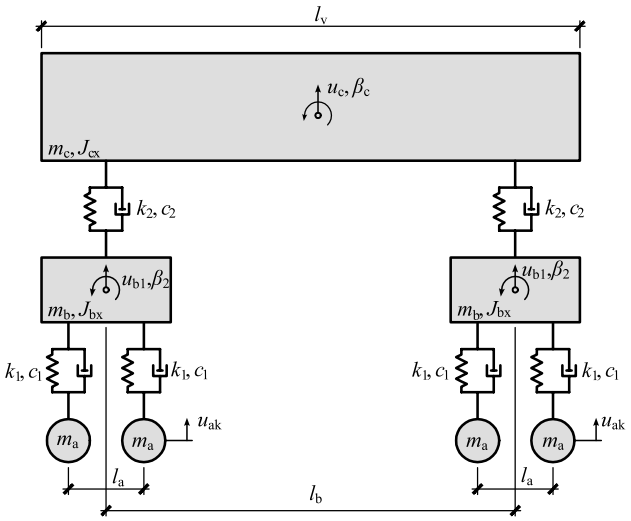

Fig. 3 2D 10-DOF vehicle model. The variables are explained in Table 3

while the primary and secondary suspensions are represented by spring and damper elements. Figure 3 shows a 2D 10-DOF vehicle model consisting of the car body,

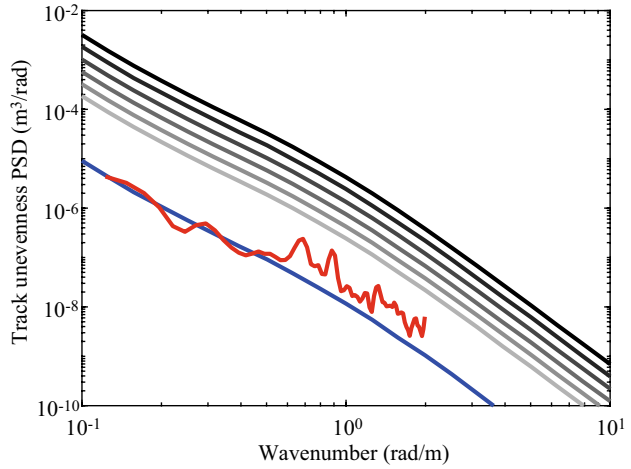

Fig. 4 One-sided PSD of the track unevenness for FRA track quality classes 1 (black) to 6 (light grey). Superimposed is the measured vertical track unevenness at the site in Lincent (red) and estimated fit (blue)

two bogies, four axles, as well as primary and secondary suspensions.

Random track unevenness is modelled as a stationary Gaussian random process characterized by its one-sided power spectral density (PSD). The spectral representation theorem is used to generate samples of track unevenness as a superposition of harmonic functions with random phase angles [36, 40]. Figure 4 shows the PSD of the unevenness for several FRA track quality classes, labelled from 1 to 6, where 1 represents the poorest and 6 the best track quality [41, 42]. Superimposed on the figure is the PSD of the vertical track unevenness measured on the high-speed track in Lincent (Belgium), as will be discussed in Sect. 5.

2.3.2 Computation of the quantities of interest

All quantities of interest defined in the empirical procedure for Detailed Vibration Assessment proposed by FRA and FTA can straightforwardly be computed with the MOTIV and TRAFFIC models.

The mean square value of the stationary part of the vibration velocity $v^2_{\mathrm{RMS}}(\boldsymbol{x}_1)$ is determined in one-third octave bands and the vibration velocity level $L_{\mathrm{v}}(\boldsymbol{x}_1)$ is defined as

$$L_{\mathrm{v}}(\boldsymbol{x}_1) = 10\log_{10}\frac{v^2_{\mathrm{RMS}}(\boldsymbol{x}_1)}{v^2_{\mathrm{ref}}}, \tag{19}$$

where v_{ref} is a reference value equal to $5\times10^{-8}\,\mathrm{m/s}$. An analytical expression for the LSTM $\mathrm{TM}_{\mathrm{L}}(\boldsymbol{X},\boldsymbol{x}_1)$ is

$$\mathrm{TM}_{\mathrm{L}}(\boldsymbol{X},\boldsymbol{x}_1) = 10\log_{10}\left[\frac{L_{\mathrm{t}}}{n_{\mathrm{a}}}\sum_{k=1}^{n_{\mathrm{a}}}\frac{\int_{\omega_1}^{\omega_2}|\mathrm{i}\omega\hat{h}_{zz}(\boldsymbol{X}_k,\boldsymbol{x}_1,\omega)|^2\,\mathrm{d}\omega}{\Delta\omega}\frac{1}{v^2_{\mathrm{ref}}}\right]. \tag{20}$$

Equation (20) represents the average value of the vibration energy transfer for all axles multiplied by the train length L_{t}. The term $\hat{h}_{zz}(\boldsymbol{X}_k,\boldsymbol{x}_1,\omega)$ is the transfer function relating the vibration at the receiver $\boldsymbol{x}_1$ in the direction $\boldsymbol{e}_z$ due to a point load at the source $\boldsymbol{X}_k$ in the direction $\boldsymbol{e}_z$, and is first averaged over the frequency band $[\omega_1,\omega_2]$ with bandwidth $\Delta\omega$, then summed over the total number of axles. This expression is dependent on, yet relatively insensitive to, the exact position of the axles and the number of source points considered [37].

Following the empirical procedure for Detailed Vibration Assessment, the force density $L_{\mathrm{F}}(\boldsymbol{X},\boldsymbol{x}_1)$ is computed indirectly as the difference between the vibration velocity level $L_{\mathrm{v}}(\boldsymbol{x}_1)$ and the LSTM $\mathrm{TM}_{\mathrm{L}}(\boldsymbol{X},\boldsymbol{x}_1)$:

$$L_{\mathrm{F}}(\boldsymbol{X},\boldsymbol{x}_1) = L_{\mathrm{v}}(\boldsymbol{x}_1) - \mathrm{TM}_{\mathrm{L}}(\boldsymbol{X},\boldsymbol{x}_1). \tag{21}$$

Under the assumption of fixed, incoherent and equal axle loads, the force density can also be expressed as [30]

$$L_{\mathrm{F}}(\boldsymbol{X}) \simeq 10\log_{10}\left[\frac{n_{\mathrm{a}}}{L_{\mathrm{t}}}\frac{g^2_{\mathrm{dRMS}}}{F^2_{\mathrm{ref}}}\right], \tag{22}$$

where F_{ref} is a reference value equal to $1\,\mathrm{N}/\sqrt{\mathrm{m}}$. Equation (22) represents the mean square force per unit length applied by the axles at the wheel/rail contact at fixed positions. It is calculated based on the spectrum g_{dRMS} of a single dynamic axle load, obtained with Eq. (17) and expressed in one-third octave bands, and the ratio of the number of axles n_{a} to the train length L_{t}. The term g_{dRMS} only contains the dynamic component of the axle load. The static axle load results in a quasi-static contribution to the free field response and cannot be written in the form of Eq. (1). This quasi-static contribution is only significant at low frequencies close to the track and can thus be neglected. Expression (22) for the force density is independent of the separation distance of the source and receiver, as a result of the approximations introduced in its derivation. It is referred to as the "direct" method of calculating the force density, cf. the "indirect" method given in Eq. (21).

2.4 Hybrid prediction schemes

As each of the quantities of interest (force density, LSTM) can be measured or predicted, hybrid prediction schemes can be defined, in which empirical and numerical data are combined following Eq. (2), providing more flexibility and applicability than purely experimental or numerical models [30–32, 36, 37].

Hybrid model 1 combines a numerical source model with an empirical propagation term. The force density $L_{\mathrm{F}}^{\mathrm{NUM}}(\boldsymbol{X})$ can be computed directly, resulting in

$$L_{\mathrm{v}}^{\mathrm{HYB}}(\boldsymbol{x}_1) = L_{\mathrm{F}}^{\mathrm{NUM}}(\boldsymbol{X}) + \mathrm{TM}_{\mathrm{L}}^{\mathrm{EXP}}(\boldsymbol{X},\boldsymbol{x}_1). \tag{23}$$

Alternatively, the force density $L_{\mathrm{F}}^{\mathrm{NUM}}(\boldsymbol{X},\boldsymbol{x}_1)$ is computed indirectly as the difference between a predicted vibration velocity and LSTM:

$$L_{\mathrm{v}}^{\mathrm{HYB}}(\boldsymbol{x}_1) = L_{\mathrm{v}}^{\mathrm{NUM}}(\boldsymbol{x}_1) \underline{- \mathrm{TM}_{\mathrm{L}}^{\mathrm{NUM}}(\boldsymbol{X},\boldsymbol{x}_1) + \mathrm{TM}_{\mathrm{L}}^{\mathrm{EXP}}(\boldsymbol{X},\boldsymbol{x}_1)}. \tag{24}$$

The underlined term is a correction on the predicted vibration velocity level, accounting for the difference between the measured and predicted LSTM. Equations (23) and (24) are useful to assess new rolling stock or a new railway line where the force density cannot be measured.

Hybrid model 2 combines a measured force density with a predicted LSTM:

$$\begin{aligned} L_{\mathrm{v}}^{\mathrm{HYB}}(\boldsymbol{x}_1) &= L_{\mathrm{F}}^{\mathrm{EXP}}(\boldsymbol{X},\boldsymbol{x}_1) + \mathrm{TM}_{\mathrm{L}}^{\mathrm{NUM}}(\boldsymbol{X},\boldsymbol{x}_1) \\ &= L_{\mathrm{v}}^{\mathrm{EXP}}(\boldsymbol{x}_1) \underline{- \mathrm{TM}_{\mathrm{L}}^{\mathrm{EXP}}(\boldsymbol{X},\boldsymbol{x}_1) + \mathrm{TM}_{\mathrm{L}}^{\mathrm{NUM}}(\boldsymbol{X},\boldsymbol{x}_1)}. \end{aligned} \tag{25}$$

This expression combines a measured vibration velocity at the receiver $\boldsymbol{x}_1$ with a numerical adjustment of the propagation path term (underlined). This model is useful when the effect of a modification to the vibration propagation path of an existing railway is to be evaluated [31]. Examples of such modifications include open trenches [43], soft or stiff wave barriers [44, 45] and heavy masses next to the track [46], all of which have been shown to impede the transmission of waves through the soil.

In all previous expressions, the building correction factor $C_{\mathrm{b}}(\boldsymbol{x}_1,\boldsymbol{x}_{\mathrm{b}})$ was omitted for brevity. When assessing vibration in a new building close to an existing railway, for example, the following hybrid approach can be employed:

$$\begin{aligned} L_{\mathrm{v}}^{\mathrm{HYB}}(\boldsymbol{x}_{\mathrm{b}}) = {} & L_{\mathrm{F}}^{\mathrm{EXP}}(\boldsymbol{X},\boldsymbol{x}_1) \\ & + \mathrm{TM}_{\mathrm{L}}^{\mathrm{EXP}}(\boldsymbol{X},\boldsymbol{x}_1) + C_{\mathrm{b}}^{\mathrm{NUM}}(\boldsymbol{x}_1,\boldsymbol{x}_{\mathrm{b}}), \end{aligned} \tag{26}$$

while in case of an existing building next to a new-built railway, an empirical building correction factor $C_{\mathrm{b}}^{\mathrm{EXP}}(\boldsymbol{x}_1,\boldsymbol{x}_{\mathrm{b}})$ can be added to Eqs. (23) or (24).

3 Hybrid vibration prediction tool developed in SILVARSTAR

The hybrid vibration prediction tool developed in SILVARSTAR follows the methodology outlined in Sect. 2, offering the following alternatives: numerical prediction, empirical prediction and hybrid prediction, with numerical or empirical assessment of the force density or LSTM. The option to characterize the source with a reference vibration level next to the track—instead of a force density—and the propagation by means of a difference in LSTMs, as per Eq. (11), is also available.

3.1 Numerical prediction model

The numerical prediction model incorporated in SILVARSTAR's hybrid vibration prediction tool is inspired by the models MOTIV and TRAFFIC. It is developed in MATLAB, building further on Vibratec's GroundVIB model [33]. The model computes dynamic axle loads, forces transmitted to the ground and free field vibration for trains running on tracks at grade and in tunnels. It consists of a semi-analytical train–track–(tunnel–)soil interaction model formulated in the wavenumber-frequency domain.

The vehicle is represented by an MDOF model (Fig. 3). The ballasted or slab track is modelled by Euler–Bernoulli beams for the rails (and slab) with resilient layers for rail pads, under sleeper pads, ballast and under ballast or slab mat.

Both tracks at grade and tracks in (circular) tunnels are considered. In order to reduce computation times, track–soil and track–tunnel–soil impedance functions, as well as transfer functions from track to free field, are pre-computed in the wavenumber-frequency domain for selected track width, tunnel diameter and embedment depth, soil characteristics and receiver locations. Further detail is given in Sect. 3.2.

The dynamic axle loads are obtained by solving the train–track–soil interaction problem in the frequency domain, considering rail and wheel unevenness. The ground response is calculated in the wavenumber-frequency domain using the tractions and displacements at the track–soil or tunnel–soil interface and the pre-computed transfer functions; the response in the spatial-frequency domain is obtained by evaluation of the inverse wavenumber integrals. The response due to a train passage is obtained by summation of all axle contributions. In the vibration prediction tool, a number of modelling simplifications are made in order to reduce computation time, as will be discussed further in Sect. 4.

3.2 Numerical database

The hybrid vibration prediction tool is provided with an extensive numerical database [47, 48] to enhance user friendliness and computational efficiency.

- **Vehicle properties**. for different types of train can be selected from the database: urban tram with mono-bloc or resilient wheels, metro, IC train, high-speed train and

freight train [47]. Alternatively, vehicle properties can be introduced as numerical values.

- **Track properties**. for different types of ballasted and slab track can be selected from a database, e.g. ballasted track, ballasted track with soft rail pads or under sleeper pads and urban and main-line (floating) slab track [47]. Alternatively, track properties can be introduced as numerical values.
- **Track unevenness**. For the frequency range 1–80 Hz, typically of interest for the perception of ground vibration, and 20–250 Hz for the perception of ground-borne noise, and a train speed range of 10–100 m/s, the corresponding wavelengths of vertical unevenness lie within the range 0.04–100 m. Included in the database are one-third octave band spectra of FRA track unevenness (Fig. 4). The ISO 3095:2013 limit curve for rail roughness has been extrapolated for long wavelength track unevenness. The database also includes measured track unevenness spectra for ballasted and slab tracks that were obtained by combining short wavelength data measured using a Corrugation Analysis Trolley and longer wavelength data (≥ 0.5 m) obtained from routine measurements of vertical track alignments using Track Recording Coaches (Fig. 5). These cases are identified as well-maintained and smooth (typical for high-speed lines), normally maintained and not well-maintained track. This terminology is chosen for compatibility with CNOSSOS-EU [49], although the data themselves are not obtained from the database in CNOSSOS-EU. Additional data are included for the case of a ballasted freight line, a ballasted tram line and a tram line on slab track with embedded rails. Moreover, cases are included with corrugated rails together with the "normally maintained" and "not well-maintained" tracks for both track types.
- **Wheel roughness**. data are included separately in the database. The measured wheel roughness spectra in the database are given within the range 0.0315−0.8 m. They are defined depending on the braking system type as cast iron tread brakes, composite brake blocks and disc brakes, for consistency with CNOSSOS-EU [49]. Additionally, an example of measured tram wheel roughness is included. The unevenness level spectra are shown in Fig. 6.
- **Track–soil impedance and transfer functions**. from the track–soil interface to the free field are pre-computed in the wavenumber-frequency domain and stored in a data-

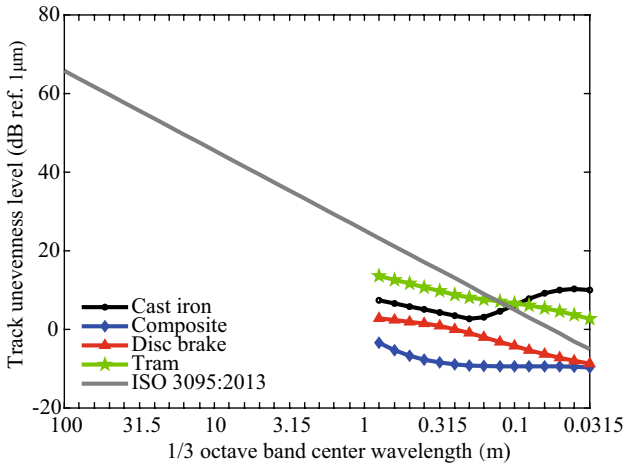

Fig. 6 Measured wheel roughness

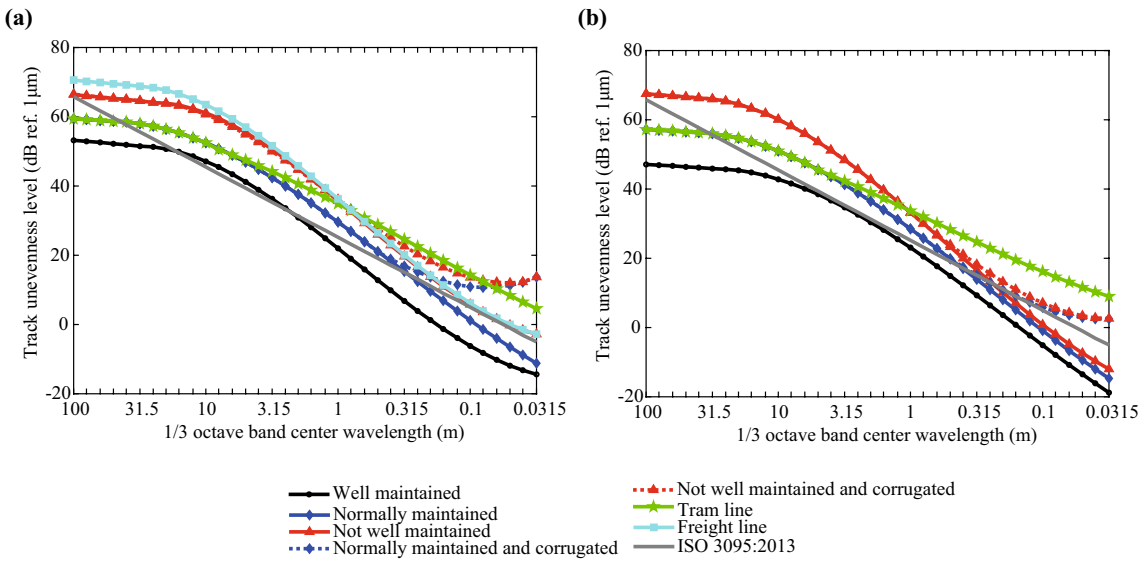

Fig. 5 Measured track unevenness for **a** ballasted and **b** slab tracks

Table 1 Dynamic soil characteristics for homogeneous soils

Soil type	C_s (m/s)	C_p (m/s)	ρ (kg/m^3)	β_s	β_p
Soft	100	200	1800	0.025	0.025
Moderately soft	140	280	1800	0.025	0.025
Medium	200	400	1800	0.025	0.025
Moderately stiff	280	560	1800	0.025	0.025
Stiff	400	800	1800	0.025	0.025

base [47]. For tracks at grade, computations are made with TRAFFIC [26] for a track width $2b$ of 3, 4.5, 6, 9 and 12 m, respectively. For tracks in tunnels, computations are made with MOTIV [25] for single-track tunnels with an outer diameter D of 4, 6 and 8 m, and twin-track tunnels with a diameter of 8, 12 and 16 m, respectively. The depth H of the tunnel centre is varied between 10 m and 20 m with an increment of 5 m. Computations are made for homogeneous soils with dynamic characteristics that accommodate five sets of soil conditions varying from soft to stiff. The dynamic soil characteristics are summarized in Table 1 in terms of the shear wave velocity C_s, dilatational wave velocity C_p, density ρ and material damping ratios β_s and β_p in shear and dilatational deformation. For surface tracks, seven layered soil cases which are typical for different European countries (Sweden, Belgium, Germany, Spain, The Netherlands, UK)—as identified in the EU FP7 project RIVAS [50]—are additionally included. The characteristics of these layered half-spaces are listed in [47] and not repeated here.

The elements of the soil impedance matrix $\tilde{\boldsymbol{K}}^{s}_{ss}(k_y, \omega)$ are stored in the database for every wavenumber and frequency [47]. The ground transfer functions define the response in the free field due to tractions at the track–soil interface and are also stored for every wavenumber and frequency [47]. For tracks at grade, TRAFFIC assumes rigid body kinematics on the track–soil interface, in terms of the vertical displacement and rotation of its centre. The ground transfer function $\tilde{h}_{sij}(x, k_y, z, \omega)$ is defined as the displacement at a receiver $\{x, z\}^T$ in the direction $\boldsymbol{e}_j$ due to a unit vertical force (or moment) on the track–soil interface corresponding to the generalized DOF i. For tracks in tunnels, MOTIV [24, 25] employs a larger number n_s of DOFs to describe the kinematics and force transfer at the track–soil interface. Rigid body kinematics are, however, easily imposed, so that similar transfer functions are computed for vertical unit loading. In the numerical model, the soil impedance matrix is coupled to the track impedance matrix to solve the track–soil interaction problem. Transfer functions in vertical and lateral direction are computed at the surface $z = 0$ at positions x from 4 m to 64 m (with a spacing Δx of 4 m) to the centre line of the track.

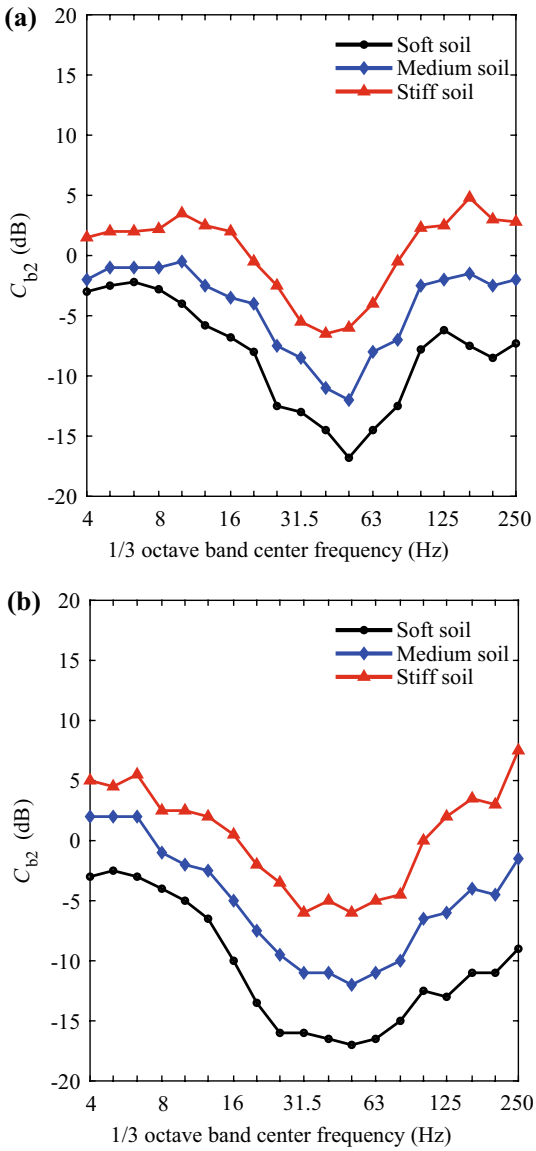

Fig. 7 Building correction factor $C_{b2}(\boldsymbol{x}_1, \boldsymbol{x}_2)$ from the soil to the building foundation for **a** single-family dwellings and **b** medium size buildings (less than 4 storeys) for soft, medium and stiff soil. The curves correspond to average values of experimental results in the RIVAS database [52]

3.3 Building correction factors

Building correction factors can be measured or computed following the general framework for Detailed Vibration Assessment proposed by FRA/FTA, as presented in Eqs. (6) or (9). Numerical predictions may account for dynamic SSI,

employing for example a 3D coupled finite element-boundary element formulation [51].

Within SILVARSTAR, the vibration velocity level $L_v(\boldsymbol{x}_b)$ inside the building is obtained from the vibration velocity level $L_v(\boldsymbol{x}_1)$ outside the building with a combination of two adjustment factors, as proposed in the EU FP7 project RIVAS on the basis of a large experimental database [52]:

$$\begin{aligned} L_v(\boldsymbol{x}_b) &= L_v(\boldsymbol{x}_1) + C_b(\boldsymbol{x}_1, \boldsymbol{x}_b) \\ &= L_v(\boldsymbol{x}_1) + C_{b2}(\boldsymbol{x}_1, \boldsymbol{x}_2) + C_{b3}(\boldsymbol{x}_2, \boldsymbol{x}_b). \end{aligned} \tag{27}$$

Dynamic SSI and attenuation or amplification within the building are accounted for in an approximate way.

The building correction factor $C_{b2}(\boldsymbol{x}_1, \boldsymbol{x}_2)$ from the ground to the building foundation depends on the type of building and the soil stiffness, and is applied to a one-third octave band spectrum in dB. Figure 7 presents building correction factors for single-family dwellings and medium size buildings (less than 4 storeys). Building correction factors are shown for soft ($C_s \leq 180$ m/s), medium (180 m/s $\leq C_s \leq 360$ m/s), and stiff ($C_s \geq 360$ m/s), soil. In most cases, attenuation can be observed when vibration is transmitted from the ground to a building foundation. The RIVAS database [52] provides insufficient experimental data to also define curves for tall buildings (more than 4 storeys). Therefore, we currently use the building correction factors for medium size buildings on soft soil for tall buildings. We are aware, however, that for tall buildings, dynamic SSI is expected to have less influence than for other building types; dynamic SSI has the largest effect for stiff (low-rise and medium) buildings founded on soft soils, for which curves are already available.

The building correction factor $C_{b3}(\boldsymbol{x}_2, \boldsymbol{x}_b)$ from the building foundation to a floor is shown in Fig. 8a. For concrete floors, an average floor resonance frequency of 31.5 Hz is observed where the building correction factor reaches a peak value of 15 dB. For wooden floors, an average floor resonance frequency of 16 Hz and peak value of 20 dB are noted.

The A-weighted sound pressure level $L_p(\boldsymbol{x}_b)$ (dB(A) ref. 2×10^{-5} Pa) inside a room of the building is obtained from the mid-span vibration velocity level $L_v(\boldsymbol{x}_b)$ (dB ref. 5×10^{-8} m/s) in the same room by applying an additional building correction factor $C_{b4}(\boldsymbol{x}_b)$ (Fig. 8b) that depends on the type of floor:

$$L_p(\boldsymbol{x}_b) = L_v(\boldsymbol{x}_b) + C_{b4}(\boldsymbol{x}_b). \tag{28}$$

It is assumed that the room is furnished [52]. For concrete floors, the building correction factor $C_{b4}(\boldsymbol{x}_b)$ is approximated as $W_A + 7$ dB, where W_A is the A-weighting curve in one-third octave bands. This approximation takes into account that both floor and ceiling radiate noise. Heavier (loaded) older wooden floors most likely behave as concrete floors.

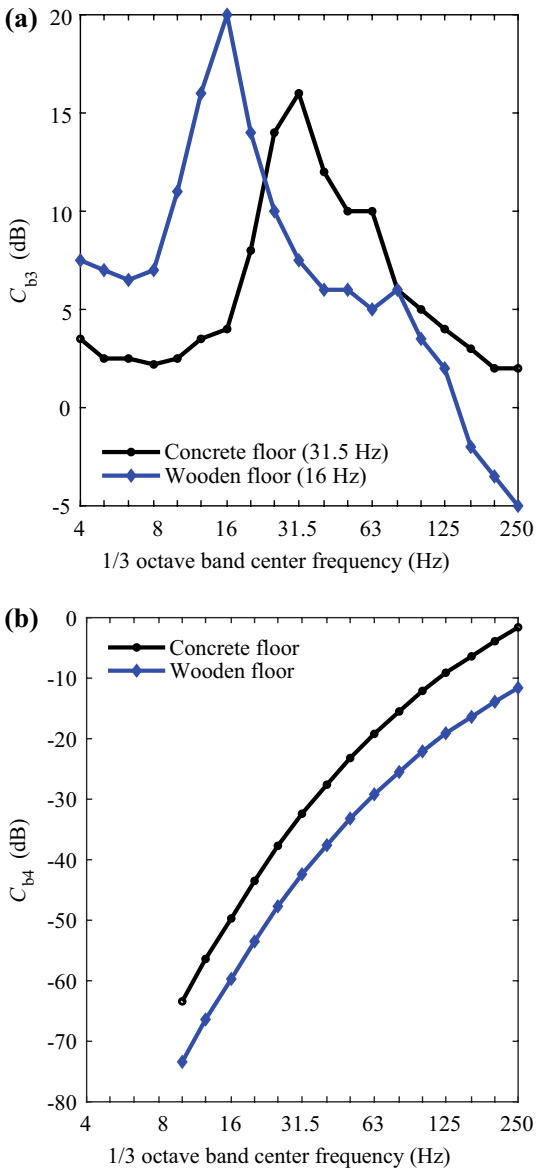

Fig. 8 Building correction factors **a** $C_{b3}(\boldsymbol{x}_2, \boldsymbol{x}_b)$ and **b** $C_{b4}(\boldsymbol{x}_b)$ for concrete and wooden floors. The curves correspond to average values of experimental results in the RIVAS database [52]

For light-weight floors, the building correction factor $C_{b4}(\boldsymbol{x}_b)$ is approximated as $W_A - 3$ dB.

The building correction factors $C_{b2}(\boldsymbol{x}_1, \boldsymbol{x}_2)$ and $C_{b3}(\boldsymbol{x}_2, \boldsymbol{x}_b)$ (Figs. 7 and 8a) are presented in one-third octave bands between 4 and 250 Hz. Perceivable vibration on floors is usually assessed in a lower frequency range up to 80 Hz, or at most 125 Hz. The reason why building correction factors are presented up to 250 Hz is that the vibration velocity level on a floor (as per Eq. 27) is the first step towards the prediction of sound pressure levels in a room as per Eq. (28). Limited availability of building correction factors presently results in relative high prediction uncertainty; therefore,

there is a great need to determine building correction factors for a much wider range of buildings and to quantify uncertainty, especially at higher frequencies where uncertain structural details and boundary conditions affect the response.

3.4 Experimental database

An experimental database of force densities, LSTMs, vibration velocity levels and input parameters (rolling stock, track, track unevenness, soil) is also provided. The following well-documented case histories are included in the database (the reader is referred to [47] for a detailed description):

- **Lincent (Belgium)**. This site is located next to the high-speed line (HSL) L2 Brussels-Köln, consisting of two classical ballasted tracks. Extensive vibration measurements were performed in the past. This case history is used to demonstrate the hybrid vibration prediction, and described in more detail in Sect. 5.
- **Heverlee (Belgium)**. This site is located along the line L1390 Leuven-Ottignies, which has two ballasted tracks with continuously welded UIC 60 rails that are supported every 0.60 m by resilient studded rubber pads on pre-stressed mono-block concrete sleepers. Measured track unevenness reveals a track of moderate-to-poor quality [53]. The alluvial soil has a 6 m thick quaternary layer of loose to dense sand on top of a tertiary formation of medium to dense sand with sandstone concretions. The ground water table is at a depth of about 8 m. Dynamic soil characteristics were identified by means of MASW, seismic refraction and SCPT, using a probabilistic Bayesian inversion framework [54]. Dynamic properties of the ballast, embankment and top soil layer were determined by comparing measured and computed track mobility [53]. Synchronized vibration measurements were performed using over 80 accelerometers mounted on sleepers, rail, along three parallel lines in the free field and at the four floors of a reinforced concrete building [32, 55, 56]. Transfer functions between track and free field were measured using an instrumented impact hammer [55, 56], with impact locations equally distributed along the track. Vibration during the passage of 143 passenger trains (electrically powered Siemens Desiro ML AM08) (77–100 km/h) and 78 freight trains (25–97 km/h) was recorded.
- **Fishbourne (UK)**. This site is located next to the West Coastway Line that runs from Portsmouth to Brighton. The track consists of two ballasted tracks in different maintenance condition with 56E1 rails supported by rubber rail pads on mono-block sleepers. Track 1 (to Brighton) (unrenewed) has stiffer rail pads than track 2 (to Portsmouth) that has been renewed and retrofitted with softer rail pads. The sleeper spacing is 0.78 m on track 1 and after renewal has been reduced to 0.65 m on track 2. The track is supported by a ballast layer and a layer of stiffened soil. Measured track unevenness reveals moderate-to-poor quality. Historical borehole archives reveal soft clays with some silt and sand content, increasing in stiffness and chalk content with depth, overlying the London Clay formation. The properties of the soil and its layered structure were determined by means of MASW tests as well as triaxial and resonant column tests on soil samples [57]. Transfer functions were measured on a 42 m long line near the tracks and used for the calculation of the vertical LSTMs. Vibration velocity level measurements correspond to British Class 377 train passages on both tracks at a speed of around 110 km/h. The data are useful for validation of models and as part of a database, but cannot be used to derive force densities as no transfer functions were measured from the track.
- **Steventon (UK)**. This site is located in Steventon next to the Great Western Main Line that runs between Didcot and Swindon. The line consists of two classical ballasted tracks on a low-height (0.7 m) embankment. Soil characteristics are available from historical borehole archives, as well as extensive in situ testing [58]. Measurements included MASW along a line perpendicular to the railway up to a distance of 42 m from the forcing point. The soil consists of clay layers; a particular feature of the site is a soft layer of clay below an intermediate layer of slightly stiffer clay. Transfer functions were measured and used for the calculation of the LSTMs. Vibration velocity level measurements correspond to a number of passages of IC 125 trains at speeds around 160 km/h and 195 km/h. Vibration was measured on the sleeper, at the top of the embankment and at several distances (from 7.5 to 80 m) from the centreline of the track. However, no transfer function measurements were made on or from the track; hence, the data could not be used to derive force densities.

The data format for the experimental database was defined based on past experience (e.g. from the FP7 project RIVAS) [47]. Users can also add new data to the experimental database. The ASCII files contain metadata describing particular properties of the experimental campaigns, together with data (force density, LSTM, vibration velocity level) in line format for each receiver [47], so that they easily can be combined with other experimental and numerical data in the hybrid vibration prediction tool.

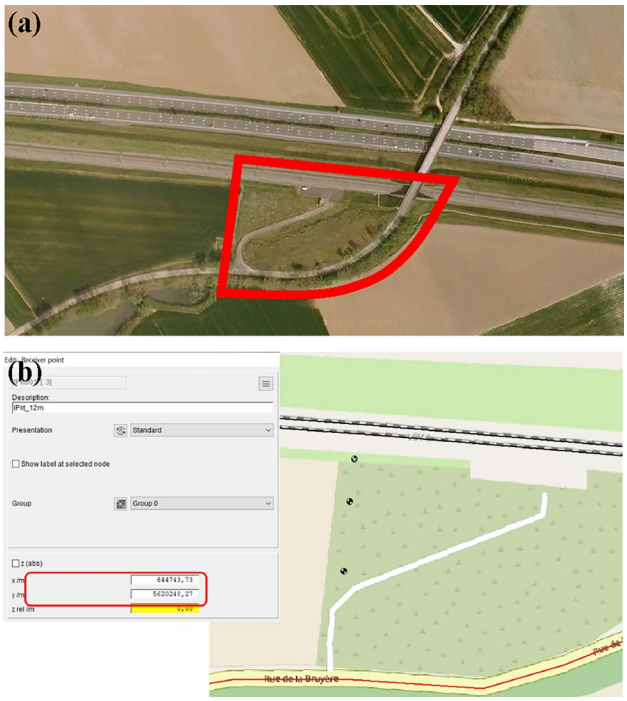

Fig. 9 **a** Satellite view of the test site in Lincent (Belgium) and **b** Open Street Map with definition of receiver points

Table 2 Properties of the ballasted track

Component	Parameter	Value
Rail UIC60	Rail positions	$l_1 = l_2 = 0.72$ m
	Cross-sectional area	$A_r = 76.70 \times 10^{-4}$ m^2
	Moment of inertia about x-axis	$I_r = 3057.1 \times 10^{-8}$ m^4
	Young's modulus	$E_r = 210 \times 10^9$ N/m^2
	Damping loss factor	$\eta_r = 0.01$
	Density	$\rho_r = 7850$ kg/m^3
Rail pad	Stiffness	$k_{rp} = 150 \times 10^6$ N/m
	Damping loss factor	$\eta_{rp} = 0.3$
Sleeper	Spacing	$d_{slp} = 0.6$ m
	Length	$l_{slp} = 2.6$ m
	Height	$h_{slp} = 0.2$ m
	Width	$b_{slp} = 0.25$ m
	Mass	$m_{slp} = 325$ kg
Ballast	Height	$h_{bal} = 0.3$ m
	Top width	$b_{balt} = 3.0$ m
	Bottom width	$b_{balb} = 3.6$ m
	Stiffness per sleeper	$k_{bal} = 500 \times 10^6$ N/m
	Poisson's ratio	$\nu_{bal} = 0.0$
	Damping loss factor	$\eta_{bal} = 0.15$
	Density	$\rho_{bal} = 1500$ kg/m^3
	Mass per unit length	$m_{bal} = 1485$ kg/m

3.5 Implementation of the vibration prediction model

The prediction model is integrated into the noise mapping software IMMI [59], and linked to a Geographical Information System (GIS), providing a software platform with Graphical User Interfaces (GUIs) that allows engineers to perform noise and vibration environmental impact studies within the same integrated environment [48, 60].

Within IMMI, the GIS software Open Street Map is used to define the track geometry. The position of the track is selected on the map, and the location of receiver points is specified. This is illustrated in Fig. 9 for the site at Lincent (Belgium). If present, any nearby buildings can also be selected as receiver locations; a building type has to be specified in order to select appropriate building correction factors.

The track, soil and vehicle properties, as well as the track unevenness are defined by the user. The user can import data from project databases dedicated to railway line development. Geotechnical data will be made importable through an interface with a GIS in a future version of the software. The use of pre-computed soil impedance and transfer functions for selected track widths and soil properties [47] considerably speeds up calculations and allows the user to quickly assess the effect of changes in train, track and soil parameters on axle loads and vibration.

When performing hybrid computations, the user needs to enter empirical data for either the force density or the LSTM. An experimental database [47] of force densities and LSTMs from well-documented measurement campaigns is also integrated in the hybrid vibration prediction tool, as was discussed in Sect. 3.4.

4 Validation of modelling assumptions

4.1 Modelling assumptions

The following modelling simplifications are incorporated in SILVARSTAR's hybrid vibration prediction tool in order to allow for fast calculations:

A1 For the computation of dynamic axle loads, the track compliance is evaluated in a stationary instead of moving frame of reference.

A2 Dynamic axle loads are applied at fixed positions instead of positions that move with the speed of the train. This low-speed approximation neglects the Doppler effect.

A3 Axle loads are assumed to be incoherent instead of coherent.

The influence of these assumptions is assessed by means of a difference in vibration velocity level $\Delta L_v(\boldsymbol{x}_1)$:

$$\Delta L_v(\boldsymbol{x}_1) = L_v^{\text{approx}}(\boldsymbol{x}_1) - L_v^{\text{ref}}(\boldsymbol{x}_1), \tag{29}$$

where $L_v^{\text{approx}}(\boldsymbol{x}_1)$ is the vibration velocity level predicted by the tool and $L_v^{\text{ref}}(\boldsymbol{x}_1)$ is a reference vibration velocity level computed with a vibration prediction model that does not incorporate the aforementioned assumptions. For this purpose, use is made of TRAFFIC [26] that was benchmarked against results from MOTIV [23–25]. In the following subsections, the assessment is made for a nominal IC train running on a ballasted track; a similar validation was performed for an IC train running on a slab track, with similar conclusions [60].

4.2 Problem outline

A ballasted track is considered for which the rails are modelled as Euler–Bernoulli beams and the rail pads are considered as continuous springs between the rails and the sleepers. The sleepers are assumed to be rigid masses, and the ballast bed is assumed to act as a layer of linear springs and dampers. The track properties are summarized in Table 2. The track unevenness is based on FRA track quality class 6 (Fig. 4).

Calculations are made for three homogeneous soils, characterized as soft, medium and stiff, and with properties as summarized in Table 1.

A nominal IC train is considered consisting of four identical vehicles. Each vehicle is represented by a 10-DOF model (Fig. 3) with properties given in Table 3. The assessment is made for three train speeds: 50 km/h, 150 km/h and

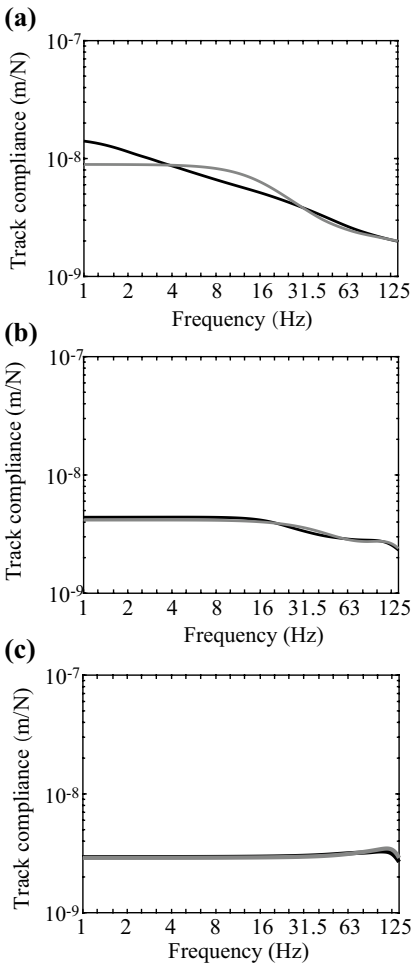

Fig. 10 Track compliance for a moving (300 km/h) (black) and fixed (grey) axle load on a ballasted track on **a** soft, **b** medium and **c** stiff soil

Table 3 Vehicle properties of the IC train

Component	Parameter	Value
Car body	Vehicle length	$l_v = 23$ m
	Mass	$m_c = 32000$ kg
	Pitching moment of inertia	$J_{cx} = 1.2 \times 10^6$ kgm^2
Bogie	Bogie spacing	$l_b = 17$ m
	Mass	$m_b = 5000$ kg
	Pitching moment of inertia	$J_{bx} = 6000$ kgm^2
Wheelset (unsprung mass)	Axle spacing	$l_a = 2.5$ m
	Mass	$m_a = 1200$ kg
	Contact stiffness (per wheel)	$k_H = 1.26 \times 10^9$ N/m
Primary suspension	Vertical stiffness per axle	$k_1 = 2 \times 10^6$ N/m
	Vertical viscous damping per axle	$c_1 = 40 \times 10^3$ Ns/m
Secondary suspension	Vertical stiffness per axle	$k_2 = 0.5 \times 10^6$ N/m
	Vertical viscous damping per axle	$c_2 = 31.6 \times 10^3$ Ns/m

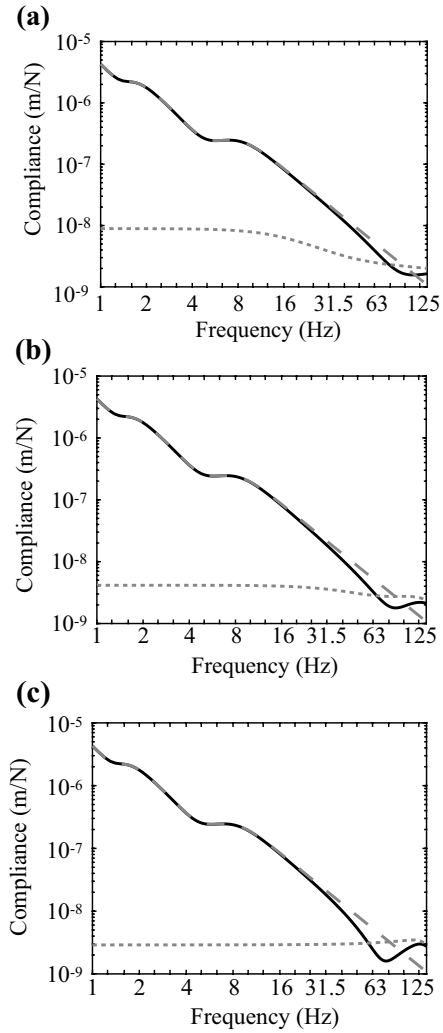

Fig. 11 Track (non-moving) (grey dotted), vehicle (grey dashed) and total (black) compliance for an axle of an IC train on a ballasted track on **a** soft, **b** medium and **c** stiff soil

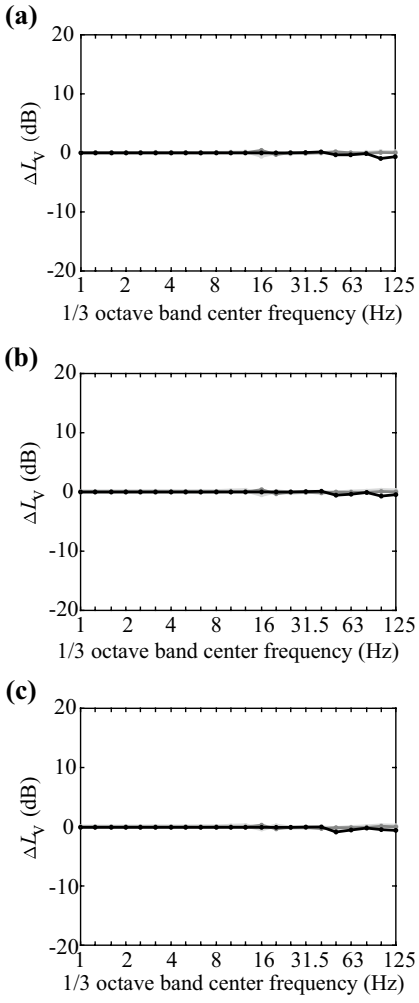

Fig. 12 Vibration velocity level difference $\Delta L_v(\boldsymbol{x}_1)$ for the track compliance in a stationary instead of a moving frame of reference at **a** 8 m, **b** 16 m and **c** 32 m for the IC train running at 300 km/h on the ballasted track on soft (light grey), medium (dark grey) and stiff (black) soil

300 km/h; the latter indeed is very high for an IC train and only introduced to enlarge the considered speed range.

4.3 Effect of train speed on track compliance

The components $\hat{C}^{\mathrm{t}}_{kl}(\omega)$ of the track compliance matrix are evaluated according to Eq. (18). When the effect of the train speed on the track compliance is disregarded (assumption A1), the computational effort to evaluate the integrals in Eq. (18) is reduced, since the transfer function $\tilde{h}^{\mathrm{t}}_{zz}(k_y, \omega)$ is an even function of the wavenumber k_y.

The track compliance was calculated for the three soil conditions considering a fixed and a moving load at the highest speed of 300 km/h (Fig. 10). There are some differences for the soft soil below about 30 Hz, while for the medium and stiff soil, the track compliances are in close agreement.

Figure 11 shows the total compliance at an axle of an IC train running on a ballasted track supported by soft, medium and stiff soil. According to Eq. (17), the total compliance is obtained as the sum of the track and vehicle compliance. As the total compliance below 60 Hz is dominated by the vehicle compliance, the observed differences in Fig. 10 have a small influence on the total compliance and the resulting dynamic axle loads. This is confirmed by Fig. 12, showing the vibration velocity level difference $\Delta L_v(\boldsymbol{x}_1)$ between the free field response calculated using the track compliance for non-moving loads and that for loads moving at 300 km/h. Even though this is the highest speed considered, the level difference is less than 1 dB for the soft soil conditions, and even smaller for stiffer soils and lower train speeds (not

shown), meaning that the influence of the moving load on the track compliance does not affect the vibration predictions in the free field.

4.4 Low-speed approximation

The low-speed approximation predicts the vibration velocity level $L_v(\boldsymbol{x}_1)$ during the stationary part of the response by assuming fixed axle positions or zero train speed (assumption A2). As a result, the Doppler shift between the receiver and the source in Eq. (15) is disregarded, resulting in the following free field velocity $\hat{v}_i(x, y, z, \omega)$:

$$\begin{aligned}\hat{v}_i(x, y, z, \omega) &= \sum_{k=1}^{n_a} \frac{1}{2\pi} \int_{-\infty}^{+\infty} \mathrm{i}\omega \tilde{h}_{zi}(x, k_y, z, \omega) \hat{g}_{dkz}(\omega) \\ &\quad \exp\left[-\mathrm{i}k_y(y - y_{k0})\right] \mathrm{d}k_y \\ &= \sum_{k=1}^{n_a} \mathrm{i}\omega \hat{h}_{zi}(x, y - y_{k0}, z, \omega) \hat{g}_{dkz}(\omega).\end{aligned} \tag{30}$$

Only the vertical component of the dynamic axle loads $\hat{g}_{dkz}(\omega)$ is accounted for. These are determined by random track unevenness and represent a random process. Therefore, the free field velocity $\hat{v}_i(x, y, z, \omega)$ is a random process as well, characterized by the one-sided PSD $\hat{S}_{v_i}(x, y, z, \omega)$:

$$\begin{aligned}\hat{S}_{v_i}(x, y, z, \omega) &= \sum_{k=1}^{n_a} \sum_{l=1}^{n_a} \omega^2 \hat{h}_{zi}(x, y - y_{k0}, z, \omega) \\ &\quad \hat{S}_{g_{kl}}(\omega) \hat{h}^*_{zi}(x, y - y_{l0}, z, \omega).\end{aligned} \tag{31}$$

The vibration velocity level $L_v(\boldsymbol{x}_1)$ is subsequently obtained by integrating this PSD in one-third octave bands.

Figure 13 shows the vibration velocity level difference $\Delta L_v(\boldsymbol{x}_1)$ at 16 m from the track between the low-speed approximation and the moving train response for three train speeds. Overall, the differences increase with increasing train speed and are more than 10 dB in individual frequency bands at the highest speed of 300 km/h. These differences mainly correspond to a redistribution of energy into different bands due to the Doppler effect, while the overall vibration level summed over all frequency bands is affected much less (as will be discussed in Sect. 4.6).

4.5 Incoherent dynamic axle loads

The final assumption A3 of incoherent axle loads implies that the coherence between two axles k and l, represented by the cross-PSD terms $\hat{S}_{g_{kl}}(\omega)$, is not taken into account in Eq. (31). These cross PSDs are oscillating functions with a period determined by the time lag $(y_{k0} - y_{l0})/v$, resulting in oscillations in the PSD $\hat{S}_{v_i}(\omega)$ that are cancelled when integrating the vibration velocity level $L_v(\boldsymbol{x}_1)$ over sufficiently wide frequency bands. Hence, the assumption of incoherent axle loads mostly affects the vibration velocity level at low frequencies where the one-third octave bands are narrower. Equation (31) becomes

$$\hat{S}_{v_i}(x, y, z, \omega) = \sum_{k=1}^{n_a} \omega^2 \mid \hat{h}_{zi}(x, y - y_{k0}, z, \omega) \mid^2 \hat{S}_{gkk}(\omega). \tag{32}$$

The vibration velocity level difference $\Delta L_v(\boldsymbol{x}_1)$ at 16 m from the track between the incoherent and coherent load case is shown in Fig. 14 for three train speeds. Largest differences at 50 km/h occur below 4 Hz; above 4 Hz, differences are less than 5 dB. At higher speeds of 150 km/h and 300 km/h, there is good agreement above 10 Hz and 20 Hz, respectively, which is where the highest response generally occurs.

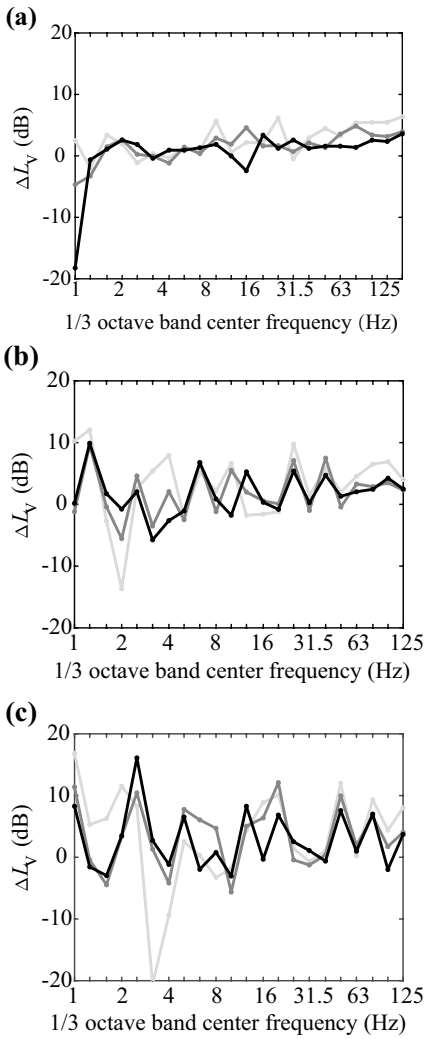

Fig. 13 Vibration velocity level difference $\Delta L_v(\boldsymbol{x}_1)$ between the low-speed approximation and the moving train response at 16 m for the IC train running at **a** 50 km/h, **b** 150 km/h and **c** 300 km/h on the ballasted track on soft (light grey), medium (dark grey) and stiff (black) soil

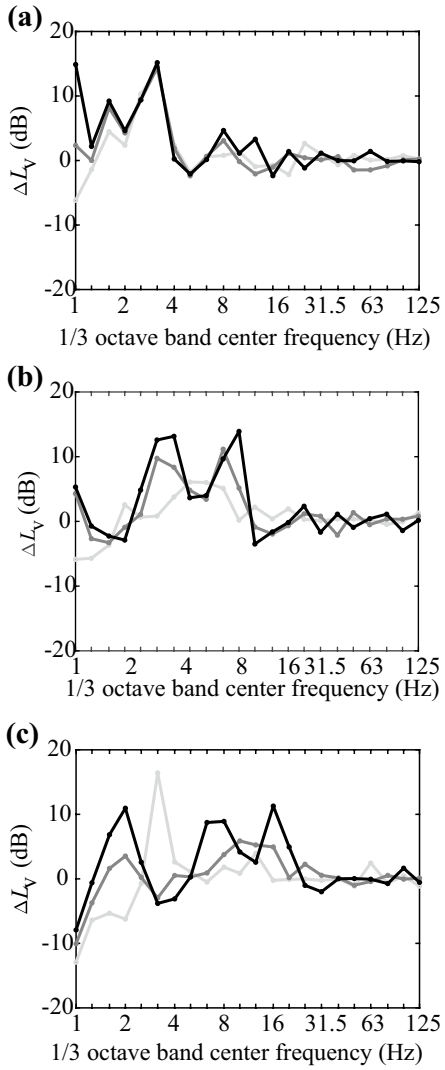

Fig. 14 Vibration velocity level difference $\Delta L_v(\boldsymbol{x}_1)$ between the incoherent load approximation and the coherent load case at 16 m for the IC train running at **a** 50 km/h, **b** 150 km/h and **c** 300 km/h on the ballasted track on soft (light grey), medium (dark grey) and stiff (black) soil

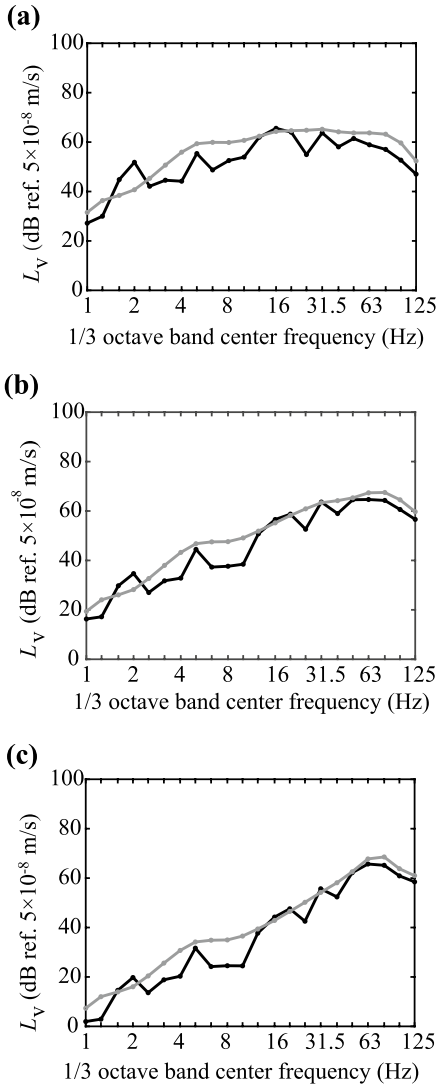

Fig. 15 Vibration velocity level $L_v(\boldsymbol{x}_1)$ at 16 m for the IC train running at 150 km/h on the ballasted track on **a** soft, **b** medium and **c** stiff soil. Results obtained with TRAFFIC for a moving train (black) and the prediction tool with approximations A1 to A3 (grey)

4.6 Overall effect of modelling assumptions

The combined effect of all three approximations at 16 m from the track is shown in Fig. 15 for the speed of 150 km/h; although there are significant differences in individual frequency bands, the spectrum shape is closely followed.

The overall vibration velocity level $L_v^{\text{overall}}(\boldsymbol{x}_1)$ is also computed by summing the contributions $L_v^j(\boldsymbol{x}_1)$ in each one-third frequency band j:

$$L_v^{\text{overall}}(\boldsymbol{x}_1) = 10 \log_{10} \sum_j 10^{\frac{L_v^j(\boldsymbol{x}_1)}{10}} \quad . \tag{33}$$

Table 4 reports the overall vibration velocity level $L_v^{\text{overall}}(\boldsymbol{x}_1)$ at 16 m from the track when modelling assumptions A1 to A3 are made. The result when none of these assumptions is made is also given, together with the overall vibration level difference. The low-speed approximation (A2) leads to the largest differences between the detailed and simplified model. The vibration level difference is generally highest for the soft soil. The overall vibration velocity level is on average 2 dB to 3 dB higher for the simplified model (A1+A2+A3) than for the detailed model. This is consistent with results presented by Verbraken [37] and demonstrates that, although the proposed modelling simplifications are a compromise to achieve efficient calculations, the differences

Table 4 Overall vibration velocity level $L_v^{\text{overall}}(\boldsymbol{x}_1)$ at 16 m from the ballasted track on soft, medium and stiff soil during the passage of the IC train at 50, 150 and 300 km/h

Train speed (km/h)	Soil type	Modelling assumptions (dB ref. 5×10^{-8} m/s)				Difference
		None	A1	A1+A2	A1+A2+A3	
50	Soft	57.9	57.9	60.8	60.8	+2.9
	Medium	57.3	57.3	60.5	59.9	+2.6
	Stiff	56.2	56.2	58.4	58.7	+2.5
150	Soft	71.8	71.7	73.7	74.6	+2.8
	Medium	71.7	71.6	74.1	74.1	+2.4
	Stiff	70.5	70.3	72.7	72.9	+2.4
300	Soft	80.3	80.3	82.7	82.8	+2.5
	Medium	80.2	80.1	82.9	82.9	+2.7
	Stiff	79.8	79.4	82.1	81.9	+2.1

Results are computed for combinations of the three modelling assumptions: track compliance in the stationary frame of reference (A1), low-speed approximation (A2) and incoherent axle loads (A3); and when none of these assumptions are made

introduced by these approximations are stronger in individual frequency bands (Fig. 15), but have much less effect on the overall vibration velocity level (Table 4). Similar conclusions can be drawn for different distances from the track [38] (not shown here), with a tendency of (slightly) increasing differences for increasing distance.

5 Demonstration of the methodology to the case history of a high-speed ballasted track

The hybrid vibration prediction tool is integrated in the noise mapping software IMMI [59] and linked to a Geographical Information System (GIS) [60]. Its use and versatility are demonstrated for the case of a ballasted track in Lincent (Belgium) on the HSL L2 Brussels-Köln (Fig. 9). Experimental results were collected on this site and incorporated in the experimental database [47], hence allowing for a demonstration and validation of the numerical and hybrid prediction capabilities of the vibration prediction tool [48, 61]. Other examples, e.g. a slab track at grade or in a tunnel, can be found in Deliverables D3.2 [48] and D3.3 [61] of the SILVARSTAR project.

5.1 Problem outline

- **Track**. The HSL L2 consists of two classical ballasted railway tracks with UIC 60 rails supported every 0.6 m by resilient studded rubber rail pads on pre-stressed mono-block concrete sleepers. The track is located in a 1 m deep cutting and supported by porphyry ballast and limestone sub-ballast layers. The depth of the ballast is 0.35 m below the sleepers. The dynamic characteristics of the rail pads, ballast and subgrade were determined from track receptance measurements [37, 40]. The track properties are summarized in Table 5.
- **Track unevenness**. The Belgian railway infrastructure manager Infrabel recorded the irregularity and alignment of both rails as well as the curvature, superelevation and

Table 5 Track properties for the Lincent site

Component	Parameter	Value
UIC60 rail	Rail positions	$l_1 = l_2 = 0.72$ m
	Bending stiffness	$E_r I_r = 6.42 \times 10^6$ Nm^2
	Mass per unit length	$\rho_r A_r = 60$ kg/m
Rail pad	Stiffness	$k_{rp} = 153.4 \times 10^6$ N/m
	Viscous damping coefficient	$c_{rp} = 13.5 \times 10^3$ Ns/m
Sleeper	Length	$l_{slp} = 2.5$ m
	Width	$b_{slp} = 0.235$ m
	Height	$h_{slp} = 0.205$ m
	Mass	$m_{slp} = 300$ kg
	Mass moment of inertia	$\rho I_{t,slp} = 157.3$ kgm^2
	Spacing	$d = 0.6$ m
Ballast	Thickness	$t_{bal} = 0.35$ m
	Top width	$b_{balt} = 3.6$ m
	Bottom width	$b_{balb} = 5.6$ m
	Mass per unit length	$m_{bal} = 1488$ kg/m
	Stiffness per sleeper	$k_{bal} = 180 \times 10^6$ N/m
	Hysteretic loss factor	$\eta_{bal} = 0.06$
Subgrade	Thickness	$t_{sub} = 1.0$ m
	Shear wave velocity	$C_{s,sub} = 300$ m/s
	Density	$\rho_{sub} = 1854$ kg/m^3

grade of the track [40]. The one-sided PSD $\tilde{S}_{u_{w/rz}}(k_y)$ of the average vertical unevenness of both rails was measured for wavelengths between 3 m and 63 m [37] and extrapolated for smaller or larger wavelengths by fitting the measured PSD to the analytical formula proposed by the FRA (Fig. 4). The fitted PSD matches the measured unevenness well for long wavelengths but is an underestimation for shorter wavelengths.

- **Dynamic soil characteristics**. Borehole sampling performed before the construction of the HSL L2 reveals the presence of a shallow 1.2 m thick quaternary silt layer, followed by a layer of fine sand up to a depth of 3.2 m. Between 3.2 and 7.5 m is a sequence of stiff layers of arenite (a sediment of a sandstone residue) embedded in clay. Below the arenite layers is a layer of clay (from 7.5 m to 8.5 m depth), followed by fine sand (from 8.5 to 10.0 m), and layers of fine sand and clay. Geophysical prospection tests (MASW, seismic refraction, SCPT) [62–65], laboratory tests (void ratio, water content, density) and bender element tests on undisturbed samples [66–68] were performed to identify the soil stratigraphy and dynamic soil characteristics (wave velocities and material damping ratios), as presented in Table 6.

  The track is situated in a 1 m deep cutting, while a 1 m deep lime stabilization was applied below the track. For the computation of the track compliance [37], the top layer in Table 6 is therefore replaced by a 1 m thick stiffer layer with shear wave velocity $C_{s,sub} = 300$ m/s, Poisson's ratio $\nu_{sub} = 1/3$ and density $\rho_{sub} = 1854$ kg/m^3 (while keeping the material damping ratios unchanged); the thickness of the second layer is reduced to 2.1 m. The soil impedance $\tilde{\boldsymbol{K}}_s(k_y, \omega)$ is computed with these modified dynamic soil characteristics, while the track–soil transfer functions $\tilde{\boldsymbol{h}}_s(x, k_y, \omega)$ are computed with the properties listed in Table 6. Both functions are included in the numerical database.
- **Rolling stock**. Four different trains are operating on the HSL L2: IC trains of type IC-A and IC-O, and Thalys and ICE high-speed trains. The operational speed of the Thalys HST is 300 km/h. We consider passages of the Thalys PKBA train, consisting of two locomotives (one at each end of the train) and 8 carriages, with a total length $L_t = 200.19$ m (between the first and last axle). Each locomotive is supported by two bogies and has four axles. The side carriages, next to the locomotive, have one independent bogie and share the second bogie with the neighbouring carriage. The six remaining central carriages share both bogies with their neighbouring carriages, resulting in an articulated train composition. The total number of bogies is 13 and, consequently, the total number of axles is 26. The vehicle length l_v, the bogie distance l_b, the axle distance l_a, the total axle mass m_t, the sprung mass m_s and the unsprung mass m_a of all carriages are summarized in Table 7 [37, 69].

5.2 Line source transfer mobility

Vibration was recorded on five parallel measurement lines, on the rail flange, the sleeper edge and in the free field (8 locations on the central line and two locations on the other lines). Transfer functions between the track and the free field were measured using an instrumented impact hammer [37, 47, 70, 71]. Impacts were applied on the edge of the sleeper at 21 locations equally distributed over a distance of 200 m, as well as on a square aluminium foundation located 5.05 m from the track at 17 positions equally distributed over a distance of 160 m.

Table 6 Dynamic soil characteristics at the Lincent site

Layer	h (m)	C_s (m/s)	C_p (m/s)	ρ (kg/m^3)	β_s	β_p
1	1.4	128	286	1800	0.044	0.044
2	2.7	176	286	1800	0.038	0.038
3	∞	355	1667	1800	0.037	0.037

Table 7 Geometrical and mass properties of the Thalys high-speed train

Component	Number of axles	l_v (m)	l_b (m)	l_a (m)	m_t (kg)	m_s (kg)	m_u (kg)
Locomotive	4	22.15	14.00	3.00	17000	14973	2027
Side carriage	3	21.84	18.70	3.00	17000	14973	2027
Central carriage	2	18.70	18.70	3.00	17000	14973	2027

Vehicle length l_v, bogie distance l_b, axle distance l_a, total axle mass m_t, sprung mass m_s and unsprung mass m_a

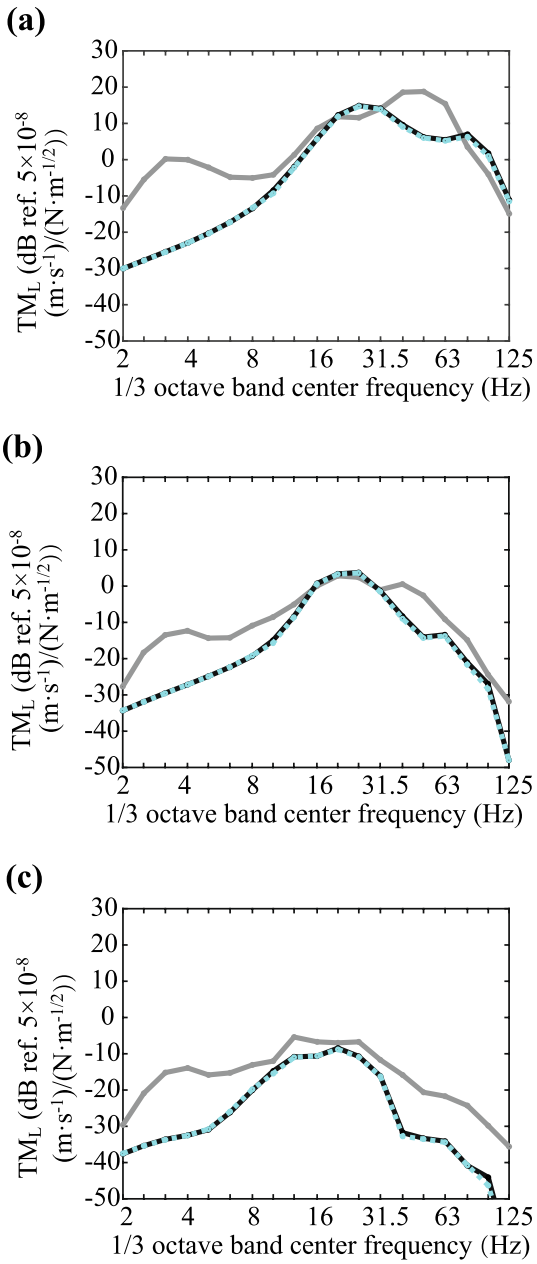

Fig. 16 Line source transfer mobility $\mathrm{TM_L}(\boldsymbol{X},\boldsymbol{x}_1)$ for the ballasted track in Lincent. Receivers are located at **a** 12 m, **b** 32 m and **c** 64 m from the track. Measured data (grey) are compared to results computed with the vibration prediction tool (black) and with TRAFFIC (cyan dotted)

The LSTM is also computed with the vibration prediction tool and with TRAFFIC; 21 source points are considered at the rail heads (0.5 N on each rail) every 10 m covering a total distance of 200 m.

Figure 16 shows the LSTM $\mathrm{TM_L}(\boldsymbol{X},\boldsymbol{x}_1)$ at 12 m, 32 m and 64 m from the track (Fig. 9b). The measured data show significant low-frequency noise below 8 Hz. At higher frequencies, the predicted and measured LSTM match relatively well for the receivers at 12 m and 32 m. At 64 m, good correspondence is observed between 10 and 30 Hz, while at higher frequencies the predictions are around 15 dB below the measured results. This is attributed to uncertainty in the estimated soil properties, particularly the material damping ratios, and to the different impact location in the experiment (on the sleeper edge) and predictions (on both rail heads) [37]. The predictions of the LSTM with the vibration prediction tool and TRAFFIC are in excellent agreement across the entire frequency range.

5.3 Vibration velocity level

Figure 17 shows the measured vibration velocity level $L_\mathrm{v}(\boldsymbol{x}_1)$ at 12 m, 32 m and 64 m from the track for five passages of the Thalys HST at speeds close to 292 km/h, together with the average vibration velocity level. The peaks at around 4 Hz (in the near field at 12 m) and 25 Hz correspond to the vehicle and axle passage frequencies, respectively. The P2 resonance is observed as a peak between 50 Hz and 63 Hz. The measured vibration velocity levels for individual passages are very close to the average vibration velocity level.

These experimental results are subsequently compared to predictions obtained with the vibration prediction tool (numerical and hybrid schemes), as well as detailed and simplified models in TRAFFIC.

- **Numerical prediction**. The vibration velocity level during a passage of the Thalys train at 292 km/h is predicted with the vibration prediction tool and compared with the experimental results, as well as with two models incorporated in TRAFFIC: a detailed model that accounts for moving dynamic and static axle loads (and hence the Doppler effect) and a simplified model with identical assumptions A1–A3 as in the vibration prediction tool (low-speed approximation and incoherent axle loads, as discussed in Sect.4).

  The predictions with the vibration prediction tool (Fig. 17) do not show peaks corresponding to the bogie and axle passages, as the dynamic axle loads are assumed to be incoherent. The P2 resonance is close to 50 Hz, which corresponds well with the measured data.

  The agreement between predictions and measurements at 12 m is very good between 10 and 20 Hz and above 80 Hz. Between 20 Hz and 80 Hz, the vibration velocity level is significantly overestimated by the vibration prediction tool. Below 10 Hz, the discrepancy is caused by omitting the contribution of the quasi-static axle loads. As the computational cost is relatively low, this contribution can be incorporated in a future version of the vibration prediction tool. Above 27 Hz (wavelengths shorter than 3 m at 292 km/h), the track unevenness is determined by extrapolation of the

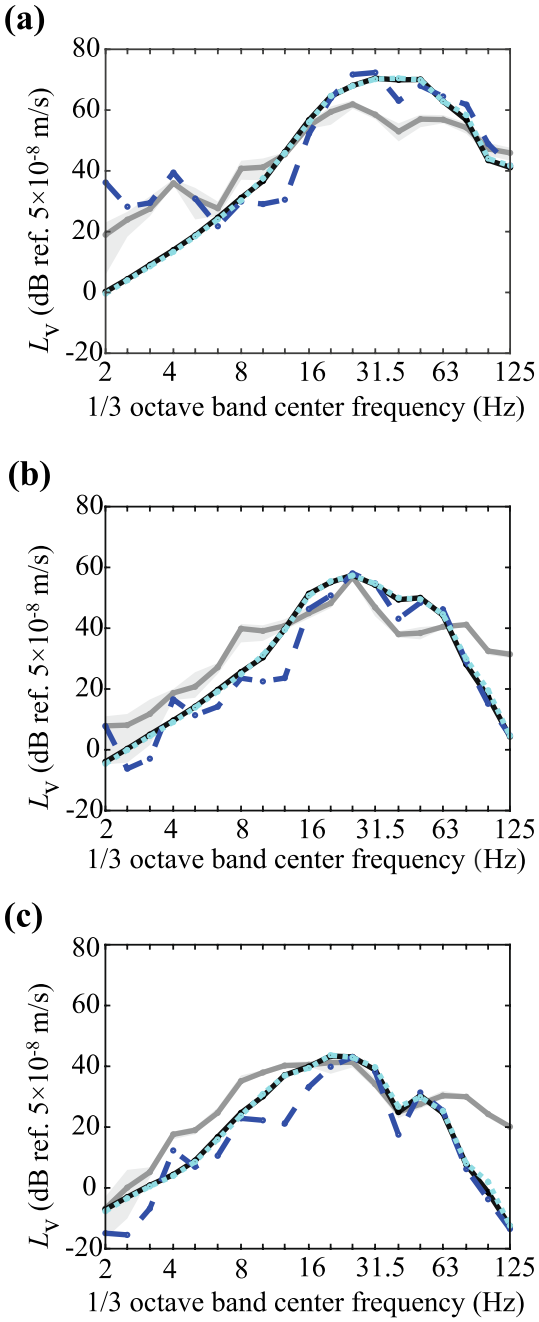

Fig. 17 Vibration velocity level $L_v(\boldsymbol{x}_1)$ during five Thalys HST passages at approximately 292 km/h on the ballasted track in Lincent (response envelope in light grey), and average vibration velocity level (dark grey). Receivers are located at **a** 12 m, **b** 32 m and **c** 64 m from the track. Results are computed with the vibration prediction tool using the numerical scheme (black) and with the detailed (blue dashed) and simplified (cyan dotted) model in TRAFFIC

measured data. Uncertainty on the dynamic soil characteristics also affects the prediction accuracy. Most probably, the material damping ratios are overestimated, resulting in a significantly lower predicted vibration velocity level at high frequencies at 32 m and 64 m.

Results obtained with the vibration prediction tool and the simplified model in TRAFFIC are in excellent agreement. Compared to results with the detailed model in TRAFFIC, the largest discrepancy is observed below 16 Hz due to the omission of the quasi-static axle loads. At higher frequencies, a smoother spectrum is obtained with the vibration prediction tool and the simplified model in TRAFFIC. Overall, spectral shapes match well.

- **Hybrid model 1**. predicts the vibration velocity level $L_v^{HYB}(\boldsymbol{x}_1)$—following Eq. (24)—as the sum of a predicted force density $L_F^{NUM}(\boldsymbol{X},\boldsymbol{x}_1)$ (difference between a predicted vibration velocity level $L_v^{NUM}(\boldsymbol{x}_1)$ and LSTM $TM_L^{NUM}(\boldsymbol{X},\boldsymbol{x}_1)$) and a measured LSTM $TM_L^{EXP}(\boldsymbol{X},\boldsymbol{x}_1)$.

  The vibration velocity levels predicted with hybrid scheme 1 (Fig. 18) show good agreement with the measurements at low frequencies. This is not expected, however, since the contribution of the quasi-static axle loads is not included in the predicted vibration velocity level $L_v^{NUM}(\boldsymbol{x}_1)$, but can be explained by the observed low-frequency noise in the measured LSTM $TM_L^{EXP}(\boldsymbol{X},\boldsymbol{x}_1)$ (Fig. 16). The vibration velocity level is overestimated around the P2 resonance between 50 Hz and 63 Hz. At 32 m and 64 m, the predicted vibration levels match better the predictions with the numerical scheme at high frequencies, due to the use of a measured LSTM.
- **Hybrid model 2**. predicts the vibration velocity level $L_v^{HYB}(\boldsymbol{x}_1)$—following Eq. (25)—as the sum of an experimental force density $L_F^{EXP}(\boldsymbol{X},\boldsymbol{x}_1)$ (difference between a measured vibration velocity level $L_v^{EXP}(\boldsymbol{x}_1)$ and LSTM $TM_L^{EXP}(\boldsymbol{X},\boldsymbol{x}_1)$) and a predicted LSTM $TM_L^{NUM}(\boldsymbol{X},\boldsymbol{x}_1)$.

  The discrepancy at low frequencies (Fig. 18) is not expected since the contribution of the quasi-static axle loads is included in the measured vibration velocity level $L_v^{EXP}(\boldsymbol{x}_1)$. It is cancelled, however, by low-frequency noise on the measured LSTM $TM_L^{EXP}(\boldsymbol{X},\boldsymbol{x}_1)$. Hybrid scheme 2 provides good prediction accuracy between 10 and 60 Hz at 12 m and 32 m; the vibration velocity spectrum clearly shows a peak around 25 Hz due to the axle passages. At higher frequencies, however, hybrid scheme 2 suffers from uncertain dynamic soil characteristics in the prediction of the LSTM $TM_L^{NUM}(\boldsymbol{X},\boldsymbol{x}_1)$, and therefore underestimates the vibration velocity level at 32 m and 64 m.

5.4 Overall vibration velocity level

Table 8 shows the overall vibration velocity level $L_v^{overall}(\boldsymbol{x}_1)$—defined according to Eq. (33) as the sum of vibration velocity levels over all one-third octave bands—at 12 m,

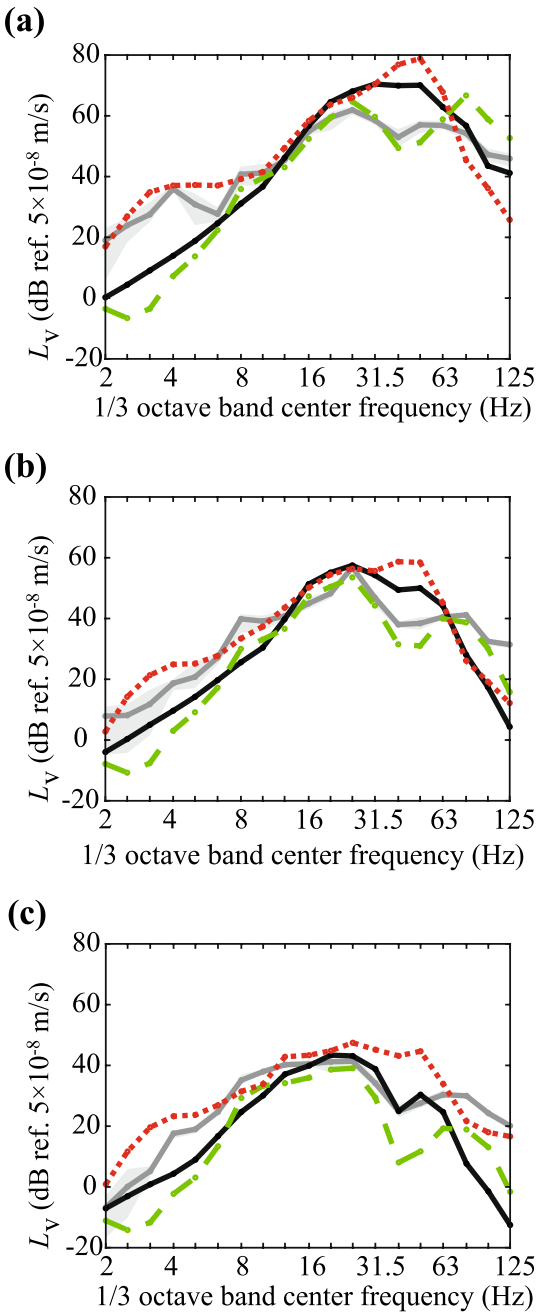

Fig. 18 Vibration velocity level $L_v(\boldsymbol{x}_1)$ during five Thalys HST passages at approximately 292 km/h on the ballasted track in Lincent (response envelope in light grey) and average vibration velocity level (dark grey). Receivers are located at **a** 12 m, **b** 32 m and **c** 64 m from the track. Results are computed with the vibration prediction tool using the numerical scheme (black) and hybrid prediction schemes 1 (red dotted) and 2 (green dashed)

32 m and 64 m. The measured vibration levels are compared to predictions with the numerical and hybrid schemes in the vibration prediction tool, and with detailed and simplified models in TRAFFIC. The overall vibration velocity level indicates whether the peak in the vibration spectrum is well predicted, whereas information on the spectral shape and prediction accuracy in individual one-third octave bands is evidently lost.

At 12 m, the discrepancy between measured and predicted overall vibration velocity level is large (between 10 and 15 dB), as expected from the one-third octave band spectra between 10 and 63 Hz (Fig. 17a). If the measured force density is used in hybrid scheme 2, overall good agreement is obtained (3.3 dB overestimation). At 32 m and 64 m, the predicted and measured overall vibration velocity levels match very well, since the peak vibration velocity level in the one-third octave band around 25 Hz is accurately predicted (Fig. 17b and c). The large underestimation of the vibration velocity level at high frequencies is not reflected in the overall vibration velocity level.

For hybrid scheme 1, the overall vibration velocity level at 32 m and 64 m is approximately 5 dB higher, mainly due to an overestimation of the vibration velocity level between 30 Hz and 63 Hz (Fig. 18b and c). The overall vibration velocity level does not reflect the improved prediction of the vibration velocity level above 63 Hz, if compared to the numerical scheme, in particular at 64 m.

Predictions with hybrid scheme 2 match the measured results relatively well; the overall vibration velocity level is slightly lower than the measured level at 32 m (−2.2 dB) and 64 m (−4.2 dB). The underestimation of the vibration velocity level below 10 Hz, and above 63 Hz at 32 m (Fig. 18b) and above 30 Hz at 64 m (Fig. 18c) does not significantly affect the overall vibration velocity level, as the velocity is low in these one-third octave bands.

5.5 Force density

The force density is determined as the difference between the measured vibration velocity level and the measured LSTM. Results are shown for five Thalys HST passages at approximately 292 km/h in Fig. 19, together with the average force density. The contribution of quasi-static axle loads is not observed in the force density extracted from the measured data due to the high level of low-frequency noise in the measured LSTM, as discussed before. The peak around 25 Hz corresponding to the axle passage frequency is clearly observed in the spectrum. The P2 resonance, which was observed in the measured vibration velocity levels between 50 and 63 Hz (Fig. 17), is not visible in the force density. The experimental force densities at 12 m and 32 m match each other relatively well, while the spectral shape of the force density at 64 m deviates, mainly at high frequencies.

The large discrepancy between the measured and predicted force density is attributed to a combination of aforementioned factors: uncertainty on the dynamic soil characteristics, extrapolation of the track unevenness for wavelengths shorter than 3 m and measurement noise. The

Table 8 Overall vibration velocity level $L_v^{\text{overall}}(\boldsymbol{x}_1)$ at 12, 32 and 64 m from the ballasted track in Lincent during the passage of the Thalys train at 292 km/h

Distance (m)	Measured (average)	Vibration prediction tool (numerical)	Vibration prediction tool (hybrid 1)	Vibration prediction tool (hybrid 2)	TRAFFIC (detailed)	TRAFFIC (simplified)
12	67.0	75.4 (+8.4)	81.4 (+14.4)	70.3 (+3.3)	76.8 (+9.8)	76.4 (+9.4)
32	58.5	61.6 (+3.1)	64.0 (+5.5)	56.3 (−2.2)	60.9 (+2.4)	61.8 (+3.3)
64	48.1	48.3 (+0.2)	53.0 (+4.9)	43.9 (−4.2)	46.1 (−2.0)	48.4 (+0.3)

Results are computed with the vibration prediction tool (numerical and hybrid schemes) and with TRAFFIC (detailed and simplified models), and are compared to the average of the measured vibration levels

predictions with the vibration prediction tool and the simplified model in TRAFFIC are, however, in good agreement.

6 Conclusion

We presented a hybrid prediction tool for railway-induced vibration, that is inspired by modern vibration standards and guidelines. The vibration velocity level in a building in each frequency band is written as the sum of a force density, a line source transfer mobility and a building correction factor, characterizing the source, propagation path and receiver. Such approach is very attractive for use in engineering consultancy, as each of the quantities of interest can be represented by numerical predictions or by experimental data.

The numerical prediction model incorporated in the hybrid prediction tool is inspired by state-of-the-art prediction models MOTIV and TRAFFIC, taking full advantage of the translational invariance of tracks and tunnels in horizontally layered soils. In order to speed up calculations, soil impedance and transfer functions were pre-computed for a wide range of soil conditions. Additional modelling simplifications (evaluation of track compliance in a stationary frame of reference; application of dynamic axle loads at fixed positions; incoherent axle loads) were made to achieve efficient calculations. Extensive validation was performed for the case of a nominal IC train running at three speeds on a ballasted track, supported by a soft, medium or stiff soil. The assumptions of fixed and incoherent axle loads have the largest influence on prediction accuracy, resulting in a redistribution of energy into different frequency bands, with larger differences at higher train speeds. The overall vibration velocity level was found to be overestimated by maximum 3 dB for all cases considered.

The experimental database embedded in the hybrid prediction model presently incorporates data collected on 4 sites in Belgium and the UK. Measurements of LSTM and vibration velocity level on the HSL L2 Brussels-Köln in Lincent were used for approval testing of the numerical as well as both hybrid prediction schemes. Hybrid scheme 1 (predicted force density, measured LSTM) results in an overestimation of the vibration velocity level around the P2 resonance between 50 and 63 Hz; at larger distance, good prediction accuracy is obtained at higher frequencies due to the use of a measured LSTM. Hybrid scheme 2 (measured force density, computed LSTM) provides good accuracy between 10 and 60 Hz at medium distance, but underestimates the vibration velocity level in the far field at frequencies above 40 Hz, which is due to uncertain dynamic soil characteristics in the prediction of the LSTM. Overall vibration velocity levels are well predicted by all prediction schemes at 32 m and 64 m from the track.

The proposed hybrid prediction model offers wide modelling flexibility at each stage of the design process. Embedding it in the existing noise mapping software IMMI simplifies the modelling process and facilitates interfacing with GIS. The tool enables the assessment of vibration levels for both large-scale studies and more detailed investigations for new and upgraded railway lines.

There are several opportunities to improve the hybrid vibration prediction model. The experimental database needs to be extended with data from complementary campaigns. Great benefit can be obtained from coupling the model to available GIS soil databases, using, e.g. correlations, between cone resistance and small strain shear modulus [72, 73]. We will then also need faster calculation of soil impedance and transfer functions, in order to provide real-time predictions for any soil layering obtained from the database. Building correction factors need to be computed for a wider range of buildings, taking into consideration construction material, load-resisting systems, shape of the building plan, height, structural irregularity, walls, floors, roof and foundation type. If building taxonomy can be inferred from GIS databases, as presently set up in the Global Earthquake Model [74], this in the longer term would also require fast real-time calculation of building correction factors. The substantial model, parameter and measurement uncertainties finally call for incorporating uncertainty quantification in model predictions.

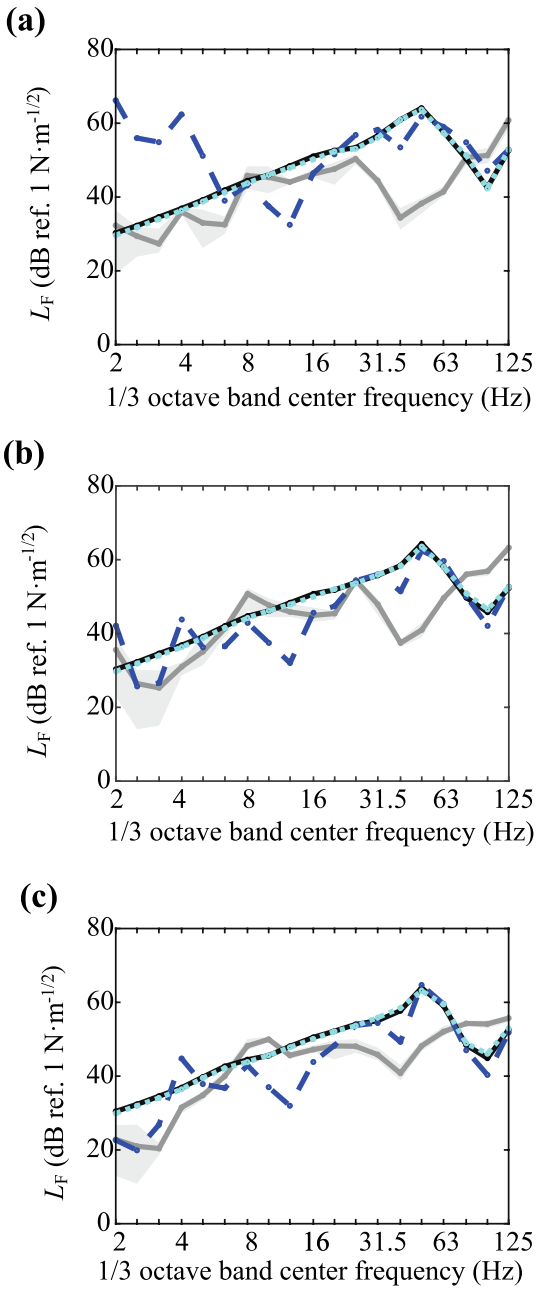

Fig. 19 Force density $L_F(\boldsymbol{X}, \boldsymbol{x}_1)$ estimated from five Thalys HST passages at approximately 292 km/h on the ballasted track in Lincent (response envelope in light grey) and average force density (dark grey). Receivers are located at **a** 12 m, **b** 32 m and **c** 64 m from the track. Results are computed with the vibration prediction tool (black), and with the detailed (blue dashed) and simplified (cyan dotted) model in TRAFFIC

Acknowledgements This paper is the result of the project SILVA-RSTAR funded from the Shift2Rail Joint Undertaking under the European Union's Horizon 2020 Research and Innovation Programme under Grant Agreement 101015442. This financial support is gratefully acknowledged.

Declarations

References

1. European Rail Research Advisory Council (2014) Strategic rail research and innovation agenda (SSRIA). A step change in rail research and innovation. Brussels
2. Lombaert G, Degrande G, François S et al (2015) Ground-borne vibration due to railway traffic. In: Nielsen JCO, Anderson D, Gautier PE (eds) Proceedings of the 11th international workshop on railway noise, Uddevalla, pp 253–287
3. Thompson DJ, Kouroussis G, Ntotsios E (2019) Modelling, simulation and evaluation of ground vibration caused by rail vehicles. Veh Syst Dyn Int J Veh Mech Mobil 57(7):936–983
4. International Organization for Standardization (2005) 14837-1:2005 mechanical vibration-ground-borne noise and vibration arising from rail systems-part 1: general guidance
5. Nelson J, Saurenman H (1987) Prediction procedure for rail transportation groundborne noise and vibration. Transp Res Rec J Transp Res Board 1143:26–35
6. Hanson CE, Ross JC, Towers DA (2012) High-speed ground transportation noise and vibration impact assessment. Technical report DOT/FRA/ORD-12/15, Federal Railroad Administration, U.S. Department of Transportation, Washington
7. Quagliata A, Ahearn M, Boeker E et al (2018) Transit noise and vibration impact assessment manual. FTA 0123, Federal Transit Administration, U.S. Department of Transportation
8. Metrikine AV, Popp K (2000) Steady-state vibrations of an elastic beam on a visco-elastic layer under moving load. Arch Appl Mech 70(6):399–408
9. Metrikine AV, Vrouwenvelder ACWM (2000) Surface ground vibration due to a moving train in a tunnel: two-dimensional model. J Sound Vib 234(1):43–66
10. Sheng X, Jones CJC, Petyt M (1999) Ground vibration generated by a harmonic load acting on a railway track. J Sound Vib 225(1):3–28
11. Sheng X, Jones CJC, Petyt M (1999) Ground vibration generated by a load moving along a railway track. J Sound Vib 228(1):129–156
12. Yang YB, Hung HH (2008) Soil vibrations caused by underground moving trains. J Geotech Geoenviron Eng 134(11):1633–1644

13. Yang YB, Hung HH (2009) Wave propagation for train-induced vibrations. World Scientific, Singapore
14. François S, Schevenels M, Lombaert G et al (2012) A 2.5D displacement based PML for elastodynamic wave propagation. Int J Numer Methods Eng 90(7):819–837
15. Andersen L (2014) Influence of dynamic soil-structure interaction on building response to ground vibration. In: Numerical methods in geotechnical engineering. CRC Press, Boca Raton
16. François S, Schevenels M, Lombaert G et al (2010) A 2.5D coupled FE–BE methodology for the dynamic interaction between longitudinally invariant structures and a layered halfspace. Comput Methods Appl Mech Eng 199(23–24):1536–1548
17. Jean P (2015) A 3D FEM/BEM code for ground–structure interaction: Implementation strategy including the multi-traction problem. Eng Anal Bound Elements 59:52–61
18. Papadopoulos M, François S, Degrande G et al (2018) The influence of uncertain local subsoil conditions on the response of buildings to ground vibration. J Sound Vib 418(4):200–220
19. Paolucci R, Spinelli D (2006) Ground motion induced by train passage. J Eng Mech 132(2):201–210
20. Triepaischajonsak N, Thompson DJ (2015) A hybrid modelling approach for predicting ground vibration from trains. J Sound Vib 335:147–173
21. Qu S, Yang J, Zhu S, Zhai W et al (2021) A hybrid methodology for predicting train-induced vibration on sensitive equipment in far-field buildings. Transp Geotech 31:100682
22. Qu S, Yang J, Feng Y et al (2022) Ground vibration induced by maglev trains running inside tunnel: Numerical modelling and experimental validation. Soil Dyn Earthq Eng 157:107278
23. Sheng X, Jones CJC, Thompson DJ (2004) A theoretical model for ground vibration from trains generated by vertical track irregularities. J Sound Vib 272(3–5):937–965
24. Ntotsios E, Thompson D, Hussein M (2017) The effect of track load correlation on ground-borne vibration from railways. J Sound Vib 402(sup1):142–163
25. Ntotsios E, Thompson DJ, Hussein MFM (2019) A comparison of ground vibration due to ballasted and slab tracks. Transp Geotech 21:100256
26. Lombaert G, François S, Degrande G (2012) TRAFFIC Matlab toolbox for traffic induced vibrations. Report BWM-2012-10. Department of Civil Engineering, KU Leuven
27. Forrest JA, Hunt HEM (2006) A three-dimensional tunnel model for calculation of train-induced ground vibration. J Sound Vib 294(4–5):678–705
28. Hussein MFM, Hunt HEM (2007) A numerical model for calculating vibration from a railway tunnel embedded in a full-space. J Sound Vib 305(3):401–431
29. Hussein MFM, Hunt HEM (2007) The PiP model, a software application for calculating vibration from underground railways. In: 14th International congress on sound and vibration, Cairns
30. Verbraken H, Lombaert G, Degrande G (2011) Verification of an empirical prediction method for railway induced vibrations by means of numerical simulations. J Sound Vib 330(8):1692–1703
31. Kuo KA, Verbraken H, Degrande G et al (2016) Hybrid predictions of railway induced ground vibration using a combination of experimental measurements and numerical modelling. J Sound Vib 373:263–284
32. Kuo KA, Papadopoulos M, Lombaert G et al (2019) The coupling loss of a building subject to railway induced vibrations: Numerical modelling and experimental measurements. J Sound Vib 442:459–481
33. Nelain B, Vincent N, Reynaud E (2021) Towards hybrid models for the prediction of railway induced vibration: numerical verification of two methodologies. In: Noise and vibration mitigation for rail transportation systems. Springer, Cham
34. Connolly DP, Marecki GP, Kouroussis G et al (2016) The growth of railway ground vibration problems—a review. Sci Total Environ 568:1276–1282
35. Silvarstar Project. Shift2Rail joint undertaking. http://www.silvarstar.eu. Accessed Sep 22 2023
36. Degrande G, Lombaert G, Ntotsios E et al (2021) State-of-the-art and concept of the vibration prediction tool. EU H2020 Project SILVARSTAR, GA 101015442, Deliverable D1.1
37. Verbraken H (2013) Prediction of railway induced vibration by means of numerical, empirical, and hybrid methods. Dissertation, Catholic University of Leuven
38. Reumers P, Degrande G, Lombaert G et al (2022) Validation of the prototype vibration prediction tool against documented cases. EU H2020 Project SILVARSTAR, GA 101015442, Deliverable D1.3
39. Stiebel D, Brick H, Garburg R et al (2020) Specification of model requirements including descriptors for vibration evaluation. FINE2 project GA-881791, Deliverable D8.1
40. Lombaert G, Degrande G, Kogut J et al (2006) The experimental validation of a numerical model for the prediction of railway induced vibrations. J Sound Vib 297(3–5):512–535
41. Hamid A, Yang TL (1981) Analytical description of track-geometry vibrations. Transp Res Rec 838:19–26
42. Garg VK, Dukkipati RV (1984) Dynamics of railway vehicle systems. Academic Press, Toronto
43. Woods RD (1968) Screening of surface wave in soils. J Soil Mech Found Div 94(4):951–979
44. Massarsch KR (2005) Vibration isolation using gas-filled cushions. In: Proceedings of the geo-frontiers 2005 congress. Austin, pp 1–20
45. Kattis SE, Polyzos D, Beskos DE (1999) Vibration isolation by a row of piles using a 3-D frequency domain BEM. Int J Numer Meth Engng 46(5):713–728
46. Takemiya H, Fujiwara A (1994) Wave propagation/impediment in a stratum and wave impeding block (WIB) measured for SSI response reduction. Soil Dyn Earthq Eng 13(1):49–61
47. Thompson DJ, Ntotsios E, Degrande G et al (2022) Database for vibration emission, ground transmission and building transfer functions. EU H2020 Project SILVARSTAR, GA 101015442, Deliverable D2.1
48. Nuber A, Schrauth J, Fröhling B et al (2023) Ground vibration prediction software: User's manual and tutorial examples. EU H2020 project SILVARSTAR, GA 101015442, Deliverable D3.2
49. CNOSSOS-EU database file. https://circabc.europa.eu. Accessed Nov 8 2021
50. Coulier P, Degrande G, Dijckmans A et al (2011) Scope of the parametric study on mitigation measures on the transmission path. EU FP7 project RIVAS SCP0-GA-2010-265754, Deliverable D4.1
51. Papadopoulos M (2018) Influence of dynamic SSI on the building response to ground vibration. Dissertation, Catholic University of Leuven
52. Villot M, Guigou C, Jean P, Picard N (2012) Procedures to predict exposure in buildings and estimate annoyance. RIVAS Project SCP0-GA-2010-265754, Deliverable D1.6
53. Germonpré M (2018) The effect of parametric excitation on the prediction of railway induced vibration in the built environment. Dissertation, Catholic University of Leuven
54. Verachtert R (2018) Deterministic and probabilistic determination of dynamic soil characteristics. Dissertation, Catholic University of Leuven
55. Maes K, Germonpré M, Zhang J et al (2017) Vibration measurements at the Blok D building of the administrative complex building of KU Leuven. Project OT/13/59. Report BWM-2017–11, Catholic University of Leuven

56. Kuo KA, Germonpré M, Maes K et al (2017) Processing of vibration measurements at the Blok D building of the administrative complex of KU Leuven. Project OT/13/59. Report BWM-2017–20, Catholic University of Leuven
57. Duley A (2019) Critical velocity effects on high speed railways. Dissertation, University of Southampton
58. Triepaischajonsak N, Thompson DJ, Jones CJC et al (2011) Ground vibration from trains: experimental parameter characterization and validation of a numerical model. Proc Inst Mech Eng Part F J Rail Rapid Transit 225(2):140–153
59. IMMI-The Software Solution for Noise. https://immi.woelfel.de/en/. Accessed Oct 13 2023
60. Nuber A, Schrauth J, Fröhling B et al (2023) User-friendly vibration prediction tool with GUI. EU H2020 Project SILVARSTAR, GA 101015442, Deliverable D3.1
61. Reumers P, Degrande G, Lombaert G et al (2023) Report on approval testing. EU H2020 Project SILVARSTAR, GA 101015442, Deliverable D3.3
62. Pyl L, Degrande G (2001) Determination of the dynamic soil characteristics with the SASW method at a site in Lincent. STWW Programme Technology and Economy, Project IWT-000152. Report BWM-2001–02, Catholic University of Leuven
63. Schevenels M, Lombaert G, Degrande G et al (2008) A probabilistic assessment of resolution in the SASW test and its impact on the prediction of ground vibrations. Geophys J Int 172(1):262–275
64. Badsar SA, Schevenels M, Haegeman W et al (2010) Determination of the damping ratio in the soil from SASW tests using the half-power bandwidth method. Geophys J Int 182(3):1493–1508
65. Schevenels M, Lombaert G, Degrande G (2011) Determination of the dynamic soil properties by refracted P-wave and and surface wave characterization at a site in Lincent (Belgium). Report BWM-2011–17, Catholic University of Leuven
66. Haegeman W (2001) In situ tests Retie-Waremme-Lincent. STWW Programme Technology and Economy, Project IWT-000152. Report RUG IV.1.16.3, Ghent University.
67. Karl L, Haegeman W (2004) Summary of the soil tests at the testing sites: Retie, Lincent, Waremme. Ghent University, Sint-Katelijne-Waver and Ghent
68. Karl L, Haegeman W, Degrande G (2006) Determination of the material damping ratio and the shear wave velocity with the seismic cone penetration test. Soil Dyn Earthq Eng 26(12):1111–1126
69. Lombaert G, Degrande G (2009) Ground-borne vibration due to static and dynamic axle loads of InterCity and high-speed trains. J Sound Vib 319(3–5):1036–1066
70. Verbraken H, Coulier P, Lombaert G et al (2012) Measurement of train passages and transfer functions at a site in Lincent. Report BWM-2012–05, Catholic University of Leuven
71. Verbraken H, Coulier P, Lombaert G et al (2012) Measurement of transfer functions at a site in Lincent. Report BWM-2012–07, Catholic University of Leuven
72. Andrus RD, Mohanan NP, Piratheepan P et al (2007) Predicting shear wave velocity from cone penetration resistance. In: Pitilakis K (ed) Proceedings of the 4th international conference on earthquake geotechnical engineering, Thessaloniki, pp 1454
73. Mayne PW, Rix GJ (1995) Correlations between shear wave velocity and cone tip resistance in natural clays. Soils Found 35(2):107–110
74. Brzev S, Scawthorn C, Charleson AW et al (2013) GEM building taxonomy version 2.0. GEM Technical Report 2013–02 V1.0.0, GEM Foundation, Pavia